2.7 Polyelectrolytes in Solution and at Surfaces

Roland R. Netz
Max-Planck Institute for Colloids and Interfaces, Potsdam, Germany

David Andelman
School of Physics and Astronomy Raymond and Beverly Sackler Faculty of Exact Sciences Tel Aviv University, Ramat Aviv, Israel

Abstract

This chapter deals with charged polymers (polyelectrolytes) in solution and at surfaces. The behavior of polyelectrolytes (PEs) is markedly different from that of neutral polymers. In bulk solutions, that is, disregarding the surface effect, there are two unique features to charged polymers: first, owing to the presence of long-ranged electrostatic repulsion between charged monomers, the polymer conformations are much more extended, giving rise to a very small overlap concentration and high solution viscosity. Second, the presence of a large number of counterions increases the osmotic pressure of PE solutions, making such polymers water soluble as this is of great importance to many applications. At surfaces, the same interplay between monomer–monomer repulsion and counterion degrees of freedom leads to a number of special properties. In particular, the adsorption behavior depends on both the concentration of polymers and the added salt in the bulk. We first describe the adsorption behavior of single PE molecules and discuss the necessary conditions to obtain an adsorbed layer and characterize its width. Depending on the stiffness of the PE, the layer can be flat and compressed or coiled and extended. We then proceed and discuss the adsorption of PEs from semidilute solutions. Mean-field theory profiles of PE adsorption are calculated as a function of surface charge density (or surface potential), the amount of salt in the system, and the charge fraction on the chains. The phenomenon of charge inversion is reviewed and its relevance to the formation of multilayers is explained. The review ends with a short overview of the behavior of grafted PEs.

2.7.1 Introduction

PEs are charged macromolecules that are extensively studied not only because of their numerous industrial applications but also from a purely scientific interest [1–4]. The most important property of PEs is their water solubility giving rise to a wide range of nontoxic, environmentally friendly, and cheap formulations. On the theoretical side, PEs combine the field of statistical mechanics of charged systems with the field of polymer science and offer quite a number of surprises and challenges.

The polymers considered in this review are taken as linear and long polymer chains, containing a certain fraction of electrically charged monomers. Chemically, this can be achieved, for example, by substituting neutral monomers with acidic ones. Upon contact with water, the acidic groups dissociate into positively charged protons, which bind immediately to water molecules, and negatively charged monomers. Although this process effectively charges the polymer molecules, the counterions make the PE solution electroneutral on macroscopic length scales.

The counterions are attracted to the charged polymers via long-ranged Coulomb interactions, but this physical

association typically only leads to rather loosely bound counterion clouds around the PE chains. Because PEs are present in a background of a polarizable and diffusive counterion cloud, there is a strong influence of the counterion distribution on the PE structure, as will be discussed at length in this review. Counterions contribute significantly toward bulk properties, such as the osmotic pressure, and their translational entropy is responsible for the generally good water solubility of charged polymers. In addition, the statistics of PE chain conformations are governed by intrachain Coulombic repulsion between charged monomers, resulting in more extended and swollen conformations of PEs as compared to neutral polymers.

All these factors combined are of great importance when considering PE adsorption to charged surfaces. We distinguish between physical adsorption, where chain monomers are attracted to surfaces via electrostatic or nonelectrostatic interactions, and chemical adsorption, where a part of the PE (usually the chain end) is chemically bound (grafted) to the surface. In all cases, the long-ranged repulsion of the dense layer of adsorbed PEs and the entropy associated with the counterion distribution are important factors in the theoretical description.

2.7.2 Neutral Polymers in Solution

Before reviewing the behavior of charged polymers, let us describe some of the important ideas underlying the behavior of neutral polymer chains in solution.

2.7.2.1 Flexible Chain Statistics

The chains considered in this review are either flexible or semiflexible. The statistical thermodynamics of flexible chains is well developed and the theoretical concepts can be applied with a considerable degree of confidence [5–9]. Long and flexible chains have a large number of conformations, a fact that plays a crucial role in determining their behavior in solution. When flexible chains adsorb on surfaces, they form a *diffusive* adsorption layer extending away from the surface into the solution. This is in contrast to semiflexible or rigid chains, which can form dense and compact adsorption layers.

The main parameters used to describe a flexible polymer chain are the polymerization index N, which counts the number of repeat units or effective monomers along the chain, and the Kuhn length a, being the size of one effective monomer or the distance between two neighboring effective monomers. The effective monomer size ranges from a few Å for synthetic polymers to a few nanometers for biopolymers [7]. The effective monomer size a is not to be confused with the actual size b of one chemical monomer; in general, a is greater than b owing to chain stiffening effects, as will be explained in detail later on. In contrast to other molecules or particles, a polymer chain contains not only translational and rotational degrees of freedom but also a vast number of conformational degrees of freedom. For typical polymers, different conformations are produced by torsional rotations of the polymer backbone bonds.

A simple description of flexible chain conformations is achieved with the freely jointed chain model in which a polymer consisting of $N + 1$ monomers is represented by N bonds defined by bond vectors $\mathbf{r}_j$ with $j = 1, \ldots N$. Each bond vector has a fixed length $|\mathbf{r}_j| = a$ corresponding to the Kuhn length, but otherwise is allowed to rotate freely. For the freely jointed chain

model, the monomer size b equals the effective monomer size a, $b = a$. Fixing one of the chain ends at the origin, the position of the $(k+1)$-th monomer is given by the vectorial sum

$$\mathbf{R}_k = \sum_{j=1}^{k} \mathbf{r}_j \tag{1}$$

Because two arbitrary bond vectors are uncorrelated in this simple model, the thermal average over the scalar product of two different bond vectors vanishes, $\langle \mathbf{r}_j \cdot \mathbf{r}_k \rangle = 0$ for $j \neq k$, while the mean-squared bond vector length is simply given by $\langle \mathbf{r}_j^2 \rangle = a^2$. It follows then that the mean-squared end-to-end radius is proportional to the number of monomers

$$\langle \mathbf{R}_N^2 \rangle = Na^2 \tag{2}$$

The same result is obtained for the mean quadratic displacement of a freely diffusing particle and eludes to the same underlying physical principle, namely, the statistics of Markov processes.

In Fig. 1(a) we show a snapshot of Monte-Carlo simulations of a freely jointed chain consisting of 100 monomers, each being represented by a sphere of diameter b (being equal here to a, the effective monomer size). The bar represents a length of $10b$, which according to Eq. (2) is the average distance between the chain ends. Indeed, the end-to-end radius gives a good idea of the typical chain radius.

The freely jointed chain model describes ideal Gaussian chains and does not account for interactions between monomers that are not necessarily close neighbors along the backbone. Including these interactions will give a different scaling behavior for long polymer chains. The end-to-end radius, $R = \sqrt{\langle R_N^2 \rangle}$, can be written more generally for $N \gg 1$ as

$$R \simeq aN^{\nu} \tag{3}$$

For an ideal polymer chain (no interactions between monomers), the above result implies $\nu = 1/2$. This result holds only for polymers in which the attraction between monomers (as compared with the monomer–solvent interaction) cancels the steric repulsion (which is due to the fact that the monomers cannot penetrate each other). This situation can be achieved in special solvent conditions called *theta* solvents.

More generally, polymers in solution can experience three types of solvent conditions, with theta solvent condition being intermediate between "good" and "bad" solvent conditions. The solvent quality depends mainly on the specific chemistry determining the interaction between the solvent molecules and monomers. It also can be changed by varying the temperature.

The solvent is called *good* when the monomer–solvent interaction is more favorable than the monomer–monomer one. Single polymer chains in good solvents have "swollen" spatial configurations, reflecting the effective repulsion between monomers. For good solvents, the steric repulsion dominates and the polymer coil takes a more swollen structure, characterized by an exponent $\nu \simeq 3/5$ [7]. This spatial size of a polymer coil is much smaller than the extended contour length $L = aN$ but larger than the size of an ideal chain $aN^{1/2}$. The reason for this peculiar behavior is entropy combined with the favorable interaction between monomers and solvent molecules in good solvents. As we will see later, it is the conformational freedom of polymer coils that leads to salient differences between polymer and simple liquid adsorption.

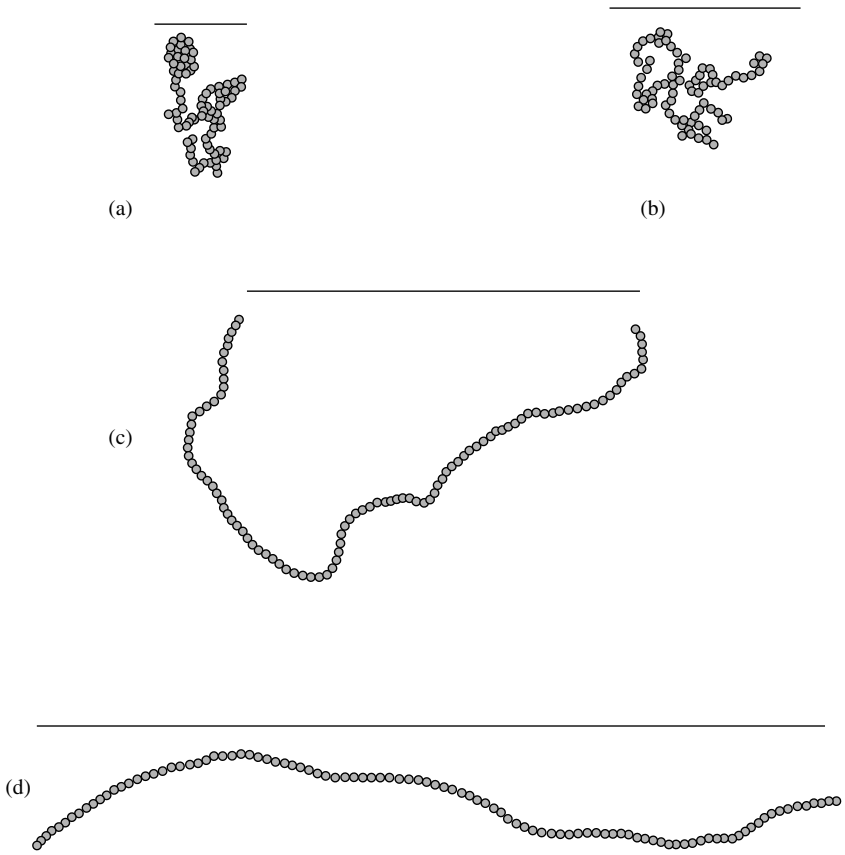

Fig. 1 Snapshots of Monte-Carlo simulations of a neutral and semiflexible chain consisting of $N = 100$ monomers of diameter b, which defines the unit of length. The theoretical end-to-end radius R is indicated by a straight bar. The persistence lengths used in the simulations are (a) $\ell_0 = 0$, corresponding to a freely jointed (flexible) chain, leading to an end-to-end radius $R/b = 10$; (b) $\ell_0/b = 2$, leading to $R/b = 19.8$; (c) $\ell_0/b = 10$, leading to $R/b = 42.4$; and (d) $\ell_0/b = 100$, leading to $R/b = 85.8$.

In the opposite case of "bad" (sometimes called *poor*) solvent conditions, the effective interaction between monomers is attractive, leading to collapse of the chains and to their precipitation from the solution (phase separation between the polymer and the solvent). It is clear that in this case, the polymer size, like any space-filling object embedded in three-dimensional space, scales as $N \sim R^3$, yielding $\nu = 1/3$.

2.7.2.2 Semiflexible Chain Statistics

Beside neglecting monomer–monomer interaction, the freely jointed chain model does not take into account the chain elasticity, which plays an important role for some polymers, and leads to more rigid structures. This stiffness can be conveniently characterized by the persistence length ℓ_0, defined as the length over which the tangent vectors at different locations on the chain are correlated. In other words,

the persistence length gives an estimate for the typical radius of curvature, while taking into account thermal fluctuations. For synthetic polymers with *trans-cis* conformational freedom of the chain backbone, the stiffness is due to fixed bond angles and hindered rotations around individual backbone bonds. This effect is even more pronounced for polymers with bulky side chains, such as poly-DADMAC, because of steric constraints, and the persistence length is of the order of a few nanometers.

Biopolymers with a more complex structure on the molecular level tend to be stiffer than simple synthetic polymers. Some typical persistence lengths encountered in these systems are $\ell_0 \approx 5\,\text{mm}$ for tubulin, $\ell_0 \approx 20\,\mu\text{m}$ for actin, and $\ell_0 \approx 50\,\text{nm}$ for double-stranded DNA. Because some of these biopolymers are charged, we will discuss at length the dependence of the persistence length on the electrostatic conditions. In some cases the main contribution to the persistence length comes from the repulsion between charged monomers.

To describe the bending rigidity of neutral polymers, it is easier to use a continuum model [6], in which one neglects the discrete nature of monomers. The bending energy (rescaled by the thermal energy, $k_\text{B}T$) of a stiff or semiflexible polymer of contour length L is given by

$$\frac{\ell_0}{2}\int_0^L \text{d}s\left(\frac{\text{d}^2\mathbf{r}(s)}{\text{d}s^2}\right)^2 \qquad (4)$$

where $\text{d}^2\mathbf{r}(s)/\text{d}s^2$ is the local curvature of the polymer. We assume here that the polymer segments are nonextendable, that is, the tangent vectors are always normalized, $|\text{d}\mathbf{r}(s)/\text{d}s| = 1$. Clearly, this continuum description will only be good if the persistence length is larger than the monomer size. The mean-squared end-to-end radius of a semiflexible chain is known and reads [6]

$$R^2 = 2\ell_0 L + 2\ell_0^2(\text{e}^{-L/\ell_0} - 1) \qquad (5)$$

where the persistence length is ℓ_0 and the total contour length of a chain is L. Two limiting behaviors are obtained for R from Eq. (5): for long chains, $L \gg \ell_0$, the chains behave as flexible ones, $R^2 \simeq 2\ell_0 L$; while for rather short chains, $L \ll \ell_0$, the chains behave as rigid rods, $R \simeq L$. Comparison with the scaling of the freely jointed chain model (Eq. 2) shows that a semiflexible chain can, for $L \gg \ell_0$, be described by a freely jointed chain model with an effective Kuhn length of

$$a = 2\ell_0 \qquad (6)$$

and an effective number of segments or monomers

$$N = \frac{L}{2\ell_0} \qquad (7)$$

In this case the Kuhn length takes into account the chain stiffness and is independent from the monomer length. This monomer size is denoted by b whenever there is need to distinguish between the monomer size b and the persistence length ℓ_0 (or Kuhn length a). In Fig. 1 we show snapshots taken from Monte-Carlo simulations of a semiflexible chain consisting of 100 polymer beads of diameter b. The persistence length is varied from $\ell_0 = 2b$ (Fig. 1b), over $\ell_0 = 10b$ (Fig. 1c), to $\ell_0 = 100b$ (Fig. 1d). Comparison with the freely jointed chain model (having no persistence length) is given in Fig. 1(a) ($a = b$, $\ell_0 = 0$). It is seen that as the persistence length is increased, the chain structure becomes more expanded. The theoretical prediction for the average end-to-end radius R (Eq. 5) is shown as the black bar on the figure and

gives a good estimate on typical sizes of semiflexible polymers.

2.7.3 Properties of Polyelectrolytes in Solution

For PEs, electrostatic interactions provide the driving force for their salient features and have to be included in any theoretical description. The reduced electrostatic interaction between two pointlike charges can be written as $z_1 z_2 v(r)$ where

$$v(r) = \frac{e^2}{k_B T \varepsilon r} \tag{8}$$

is the Coulomb interaction between two elementary charges, z_1 and z_2 are the valences (or the reduced charges in units of the elementary charge e), and ε is the medium dielectric constant. Throughout this review, all energies are given in units of the thermal energy $k_B T$. The interaction depends only on the distance r between the charges. The total electrostatic energy of a given distribution of charges is obtained from adding up all pairwise interactions between charges according to Eq. (8). In principle, the equilibrium behavior of an ensemble of charged particles (e.g. a salt solution) follows from the partition function, that is, the weighted sum over all different microscopic configurations, which – via the Boltzmann factor – depends on the electrostatic energy of each configuration. In practice, however, this route is very complicated for several reasons:

1. The Coulomb interaction (Eq. 8) is long-ranged and couples many charged particles. Electrostatic problems are typically *many-body problems*, even for low densities.
2. Charged objects in most cases are dissolved in water. Like any material, water is polarizable and reacts to the presence of a charge with polarization charges. In addition, and this is by far a more important effect, water molecules carry a permanent dipole moment that partially orients in the vicinity of charged objects. Note that for water, $\varepsilon \approx 80$, so that electrostatic interactions and self-energies are much weaker in water than in air (where $\varepsilon \approx 1$) or some other low-dielectric solvents. Still, the electrostatic interactions are especially important in polar solvents because in these solvents, charges dissociate more easily than in unpolar solvents.
3. In biological systems and most industrial applications, the aqueous solution contains mobile salt ions. Salt ions of opposite charge are drawn to the charged object and form a loosely bound counterion cloud around it. They effectively reduce or *screen* the charge of the object. The effective (screened) electrostatic interaction between two charges $z_1 e$ and $z_2 e$ in the presence of salt ions and a polarizable solvent can be written as $z_1 z_2 v_{DH}(r)$, with the Debye–Hückel (DH) potential $v_{DH}(r)$ given on the linear-response level by

$$v_{DH}(r) = \frac{\ell_B}{r} e^{-\kappa r} \tag{9}$$

The Bjerrum length ℓ_B is defined as

$$\ell_B = \frac{e^2}{\varepsilon k_B T} \tag{10}$$

and denotes the distance at which the Coulombic interaction between two unit charges in a dielectric medium is equal to thermal energy ($k_B T$). It is a measure of the distance below which the Coulomb energy is strong enough to compete with

the thermal fluctuations; in water at room temperatures, one finds $\ell_B \approx 0.7\,\text{nm}$. The exponential decay is characterized by the so-called screening length κ^{-1}, which is related to the salt concentration c_{salt} by

$$\kappa^2 = 8\pi z^2 \ell_B c_{salt} \tag{11}$$

where z denotes the valency of the screening ions ($z:z$ salt). At physiological conditions the salt concentration is $c_{salt} \approx 0.1\,\text{M}$ and for monovalent ions ($z = 1$) this leads to $\kappa^{-1} \approx 1\,\text{nm}$.

The so-called DH interaction (Eq. 9) embodies correlation effects due to the long-ranged Coulomb interactions in a salt solution using linear-response theory. In the following we estimate the range of validity of this approximation using simple scaling arguments. The number of ions that are correlated in a salt solution with concentration c_{salt} is of the order of $n \sim \kappa^{-3} c_{salt}$, where one employs the screening length κ^{-1} as the scale over which ions are correlated. Using the definition $\kappa^2 = 8\pi z^2 \ell_B c_{salt}$, one obtains $n \sim (z^2 \ell_B c_{salt}^{1/3})^{-3/2}$. The average distance between ions is roughly $r \sim c_{salt}^{-1/3}$. The typical electrostatic interaction between two ions in the solution thus is $U \sim z^2 \ell_B / r \sim z^2 \ell_B c_{salt}^{1/3}$, and we obtain $U \sim n^{-2/3}$. Using these scaling arguments, one obtains that either (1) many ions are weakly coupled together (i.e. $n \gg 1$ and $U \ll 1$) or (2) a few ions interact strongly with each other ($n \simeq U \simeq 1$). In the first case, and in the absence of external fields, the approximations leading to the DH approximation (Eq. 9) are valid.

The DH approximation forms a convenient starting point for treating screening effects, since (owing to its linear character) the superposition principle is valid and the electrostatic free energy is given by a sum over the two-body potential (Eq.9). However, we will at various points in this review also discuss how to go beyond the DH approximation, for example, in the form of the nonlinear Poisson–Boltzmann theory (see Sect. 2.7.5) or a box model for the counterion distribution (see Sect. 2.7.6).

2.7.3.1 Isolated Polyelectrolyte Chains

We discuss now the scaling behavior of a single semiflexible PE in the bulk, including chain stiffness and electrostatic repulsion between monomers. For charged polymers, the effective persistence length is increased owing to electrostatic repulsion between monomers. This effect modifies considerably not only the PE behavior in solution but also their adsorption characteristics.

The scaling analysis is a simple extension of previous calculations for flexible (Gaussian) PEs [10–12]. The semiflexible polymer chain is characterized by a bare persistence length ℓ_0 and a linear charge density τ. Using the monomer length b and the fraction of charged monomers f as parameters, the linear charge density can be expressed as $\tau = f/b$. Note that in the limit where the persistence length is small and comparable to a monomer size, only a single length scale remains, $\ell_0 \simeq a \simeq b$.

Many interesting effects, however, are obtained in the general case treating the persistence length ℓ_0 and the monomer size b as two independent parameters. In the regime where the electrostatic energy is weak, and for long enough contour length L, where $L \gg \ell_0$, a polymer coil will be formed with a radius R unperturbed by the electrostatic repulsion between monomers. According to Eq. (5), we get $R^2 \simeq 2\ell_0 L$. To estimate when the electrostatic interaction will be sufficiently

strong to swell the polymer coil, we recall that the electrostatic energy (rescaled by the thermal energy k_BT) of a homogeneously charged sphere of total charge Q and radius R is

$$W_{el} = \frac{3\ell_B Q^2}{5R} \tag{12}$$

The exact charge distribution inside the sphere only changes the prefactor of order unity and is not important for the scaling arguments. For a polymer of length L and line charge density τ, the total charge is $Q = \tau L$. The electrostatic energy of a (roughly spherical) polymer coil is then

$$W_{el} \simeq \ell_B \tau^2 L^{3/2} \ell_0^{-1/2} \tag{13}$$

The polymer length at which the electrostatic self-energy is of order k_BT, that is, $W_{el} \simeq 1$, follows as

$$L_{el} \simeq \ell_0 (\ell_B \ell_0 \tau^2)^{-2/3} \tag{14}$$

and defines the electrostatic blob size or electrostatic polymer length. We expect a locally crumpled polymer configuration if $L_{el} > \ell_0$, that is, if

$$\tau \sqrt{\ell_B \ell_0} < 1 \tag{15}$$

because the electrostatic repulsion between two segments of length ℓ_0 is smaller than the thermal energy and is not sufficient to align the two segments. This is in accord with more detailed calculations by Joanny and Barrat [11]. A recent general Gaussian variational calculation confirms this scaling result and in addition yields logarithmic corrections [12]. Conversely, for

$$\tau \sqrt{\ell_B \ell_0} > 1 \tag{16}$$

electrostatic chain–chain repulsion is already relevant on length scales comparable to the persistence length. The chain is expected to have a conformation characterized by an effective persistence length ℓ_{eff}, larger than the bare persistence length ℓ_0, that is, one expects $\ell_{eff} > \ell_0$.

This effect is clearly seen in Fig. 2, where we show snapshots of Monte-Carlo simulations of a charged chain of 100 monomers of size b each and bare persistence length $\ell_0/b = 1$ and several values of κ^{-1} and τ. The number of monomers in an electrostatic blob can be written according to Eq. (14) as $L_{el}/\ell_0 = (\tau^2 \ell_B \ell_0)^{-2/3}$ and yields for Fig. 2(a) $L_{el}/\ell_0 = 0.25$, for Fig. 2(b) $L_{el}/\ell_0 = 0.63$, for Fig. 2(c) $L_{el}/\ell_0 = 1.6$, and for Fig. 2(d) $L_{el}/\ell_0 = 4$. Accordingly, in Fig. 2(d) the electrostatic blobs consist of four monomers, and the weakly charged chain crumples at small length scales. A typical linear charge density reached with synthetic PEs such as Polystyrenesulfonate (PSS) is one charge per two carbon bonds (or, equivalently, one charge per monomer), and it corresponds to $\tau \approx 4\,\mathrm{nm}^{-1}$. Since for these highly flexible synthetic PEs the bare persistence length is of the order of the monomer size, $\ell_0 \simeq b$, the typical charge parameter for a fully charged PE therefore is roughly $\tau^2 \ell_B \ell_0 \approx 3$ and is intermediate between Fig. 2(a and b). Smaller linear charge densities can always be obtained by replacing some of the charged monomers on the polymer backbone with neutral ones, in which case the crumpling observed in Fig. 2(d) becomes relevant. Larger bare persistence lengths can be achieved with biopolymers or synthetic PEs with a conjugated carbon backbone.

The question now arises as to what are the typical chain conformations at much larger length scales. Clearly, they will be influenced by the repulsions. Indeed, in the *persistent regime*, obtained for $\tau \sqrt{(\ell_B \ell_0)} > 1$, the polymer remains locally stiff even for contour lengths larger

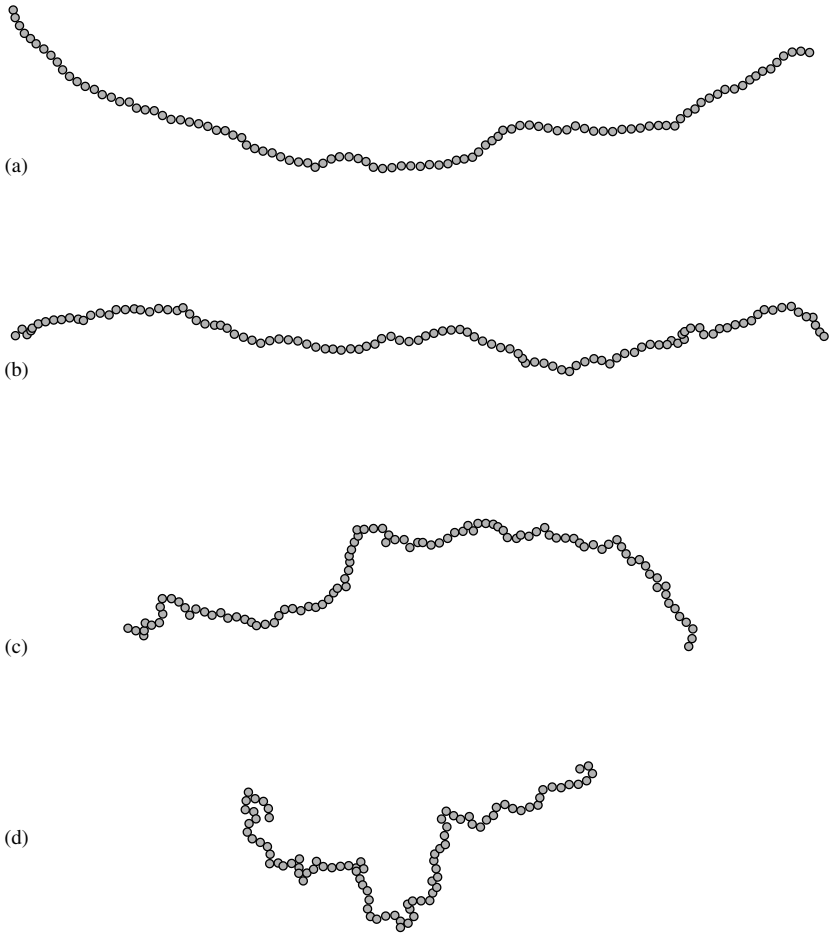

Fig. 2 Snapshots of Monte Carlo simulations of a polyelectrolyte chain of $N = 100$ monomers of size b, taken as the unit length. In all simulations the bare persistence length is fixed at $\ell_0/b = 1$, and the screening length and the charge interactions are tuned such that the electrostatic persistence length (ℓ_{OSF}) is constant and $\ell_{OSF}/b = 100$, see Eq. (18). The parameters used are (a) $\kappa^{-1}/b = \sqrt{50}$ and $\tau^2 \ell_B \ell_0 = 8$; (b) $\kappa^{-1}/b = \sqrt{200}$ and $\tau^2 \ell_B \ell_0 = 2$; (c) $\kappa^{-1}/b = \sqrt{800}$ and $\tau^2 \ell_B \ell_0 = 1/2$; and (d) $\kappa^{-1}/b = \sqrt{3200}$ and $\tau^2 \ell_B \ell_0 = 1/8$. Noticeably, the weakly charged chains crumple at small length scales and show a tendency to form electrostatic blobs.

than the bare persistence length ℓ_0, and the effective persistence length is given by

$$\ell_{\text{eff}} \simeq \ell_0 + \ell_{\text{OSF}} \tag{17}$$

The electrostatic persistence length, first derived by Odijk and independently by Skolnick and Fixman, reads [13–15]

$$\ell_{\text{OSF}} = \frac{\ell_B \tau^2}{4\kappa^2} \tag{18}$$

and is calculated from the electrostatic energy of a slightly bent polymer using the linearized DH approximation (Eq. 9).

It is valid only for polymer conformations that do not deviate too much from the rodlike reference state. The electrostatic persistence length gives a sizable contribution to the effective persistence length only for $\ell_{OSF} > \ell_0$. This is equivalent to the condition

$$\tau\sqrt{\ell_B \ell_0} > \ell_0 \kappa \qquad (19)$$

The persistent regime is obtained for parameters satisfying both conditions (16) and (19). Another regime called the *Gaussian regime* is obtained in the opposite limit of $\tau\sqrt{(\ell_B \ell_0)} < \ell_0 \kappa$.

The electrostatic persistence length is visualized in Fig. 3, in which we present snapshots of Monte-Carlo simulations of a charged chain consisting of 100 monomers of size b. The bare persistence length was fixed at $\ell_0 = b$, and the charge-interaction parameter was chosen to be $\tau^2 \ell_B \ell_0 = 2$, close to the typical charge density in experiments on fully charged synthetic PEs. The snapshots correspond to varying screening lengths of (1) $\kappa^{-1}/b = \sqrt{2}$,

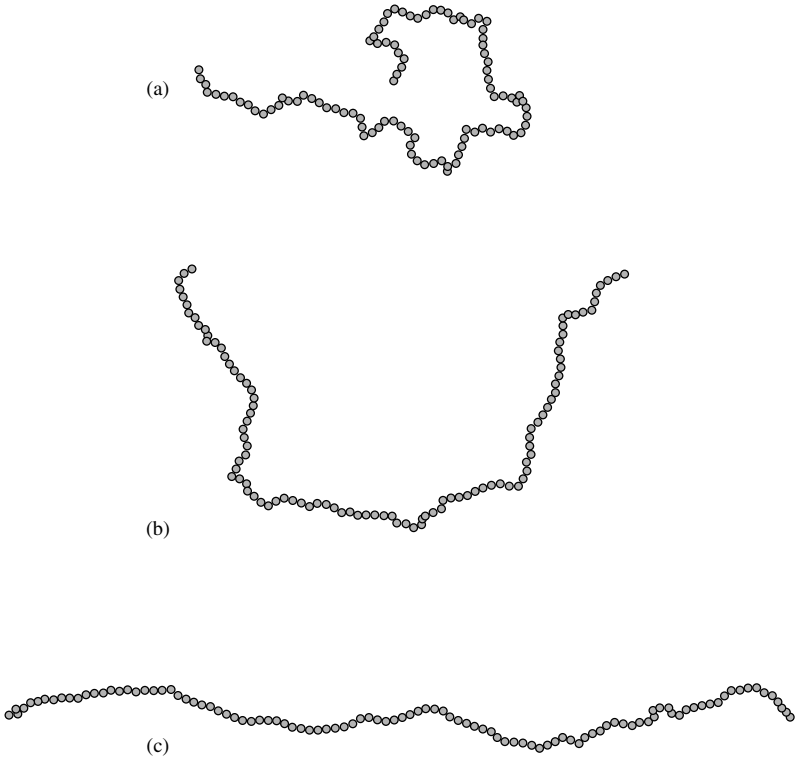

Fig. 3 Snapshots of Monte-Carlo simulations of a PE chain consisting of $N = 100$ monomers of size b. In all simulations, the bare persistence length is fixed at $\ell_0/b = 1$ and the charge-interaction parameter is chosen to be $\tau^2 \ell_B \ell_0 = 2$. The snapshots correspond to varying screening lengths of (a) $\kappa^{-1}/b = \sqrt{2}$, leading to an electrostatic contribution to the persistence length of $\ell_{OSF}/b = 1$; (b) $\kappa^{-1}/b = \sqrt{18}$, leading to $\ell_{OSF}/b = 9$; and (c) $\kappa^{-1}/b = \sqrt{200}$, leading to $\ell_{OSF}/b = 100$. According to the simple scaling principle (Eq. 17), the effective persistence length in the snapshots (a–c) should be similar to the bare persistence length in Fig. 1(b–d).

leading to an electrostatic contribution to the persistence length of $\ell_{OSF} = b$ (Fig. 3a), (2) $\kappa^{-1}/b = \sqrt{18}$, or $\ell_{OSF} = 9b$ (Fig. 3b), and (3) $\kappa^{-1}/b = \sqrt{200}$, equivalent to $\ell_{OSF} = 100b$ (Fig. 3c). According to the simple scaling principle (Eq. 17), the effective persistence length in the snapshots (Fig. 3a–c) should be similar to the bare persistence length in Fig. 1(b–d), and indeed, the chain structures in Figs. 3(c) and 1(d) are very similar. Figs. 3(a) and 1(b) are clearly different, although the effective persistence length should be quite similar, mostly because of self-avoidance effects that are present in charged chains and are discussed in detail in Sect. 2.7.3.1.2.

For the case in which the polymer crumples on length scales larger than the bare bending rigidity, that is, for $L_{el} > \ell_0$ or $\tau\sqrt{(\ell_B \ell_0)} < 1$, the electrostatic repulsion between polymer segments is not strong enough to prevent crumpling on length scales comparable to ℓ_0, but can give rise to a chain stiffening on larger length scales, as explained by Khokhlov and Khachaturian [10] and confirmed by Gaussian variational methods [12]. Figure 4 schematically shows the PE structure in this regime, where the chain on small scales consists of Gaussian blobs of chain length L_{el}, within which electrostatic interactions are not important. On larger length scales, electrostatic repulsion leads to a chain stiffening, so that the PE forms a linear array of electrostatic blobs. To quantify this effect, one defines an effective line charge density of a linear array of electrostatic blobs with blob size $R_{el} \simeq \sqrt{(\ell_0 L_{el})}$,

$$\tilde{\tau} \simeq \frac{\tau L_{el}}{R_{el}} \simeq \tau \left(\frac{L_{el}}{\ell_0}\right)^{1/2} \qquad (20)$$

Combining Eqs. (18) and (20) gives the effective electrostatic persistence length for a string of electrostatic blobs,

$$\ell_{KK} \simeq \frac{\ell_B^{1/3} \ell_0^{-2/3} \tau^{2/3}}{\kappa^2} \qquad (21)$$

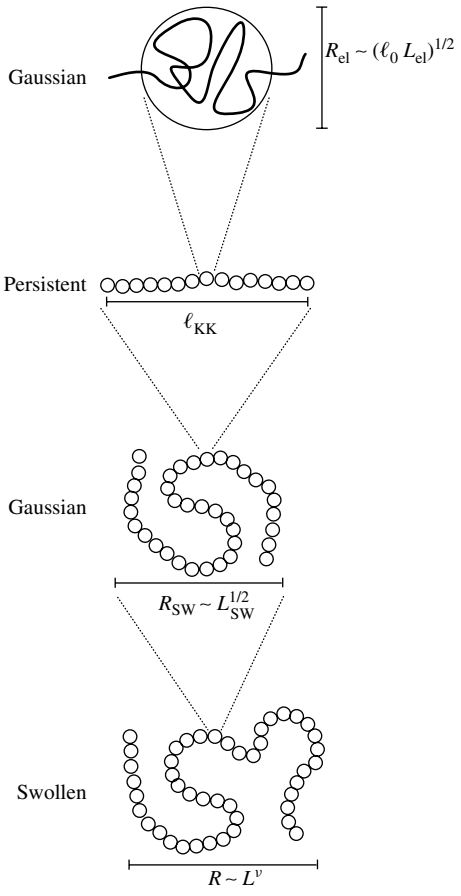

Fig. 4 Schematic view of the four scaling ranges in the Gaussian-persistent regime. On spatial scales smaller than R_{el}, the chain behavior is Gaussian; on length scales larger than R_{el} but smaller than ℓ_{KK}, the Gaussian blobs are aligned linearly. On length scales up to L_{sw}, the chain is isotropically swollen with an exponent $\nu = 1/2$, and on even larger length scales, self-avoidance effects become important and ν changes to $\nu = 3/5$.

This electrostatic stiffening is only relevant for the so-called *Gaussian-persistent regime* valid for $\ell_{KK} > R_{el}$, or equivalently

$$\tau\sqrt{\ell_B\ell_0} > (\ell_0\kappa)^{3/2} \qquad (22)$$

When this inequality is inverted, the Gaussian-persistence regime crosses over to the Gaussian one.

The crossover boundaries (Eqs. 16, 19, 22) between the various scaling regimes are summarized in Fig. 5. We obtain three distinct regimes. In the persistent regime, for $\tau\sqrt{(\ell_B\ell_0)} > \ell_0\kappa$ and $\tau\sqrt{(\ell_B\ell_0)} > 1$, the polymer takes on a rodlike structure with an effective persistence length larger than the bare persistence length and given by the OSF expression (Eq. 18). In the Gaussian-persistent regime, for $\tau\sqrt{(\ell_B\ell_0)} < 1$ and $\tau\sqrt{(\ell_B\ell_0)} > (\ell_0\kappa)^{3/2}$, the polymer consists of a linear array of Gaussian electrostatic blobs, as shown in Fig. 4, with an effective persistence length ℓ_{KK} larger than the electrostatic blob size and given by Eq. (21). Finally, in the Gaussian regime, for $\tau\sqrt{(\ell_B\ell_0)} < (\ell_0\kappa)^{3/2}$ and $\tau\sqrt{(\ell_B\ell_0)} < \ell_0\kappa$, the electrostatic repulsion does not lead to stiffening effects at any length scale.

The persistence length ℓ_{KK} was also obtained from Monte-Carlo simulations with parameters shown in Fig. 2(d), where chain crumpling at small length scales and chain stiffening at large length scales occur simultaneously [16–20]. However, extremely long chains are needed in order to obtain reliable results for the persistence length, since the stiffening occurs only at intermediate length scales and therefore fitting of the tangent–tangent correlation function is nontrivial. Nevertheless, simulations point to a different scaling than that in Eq. (21), with a dependence on the screening length closer to a linear one, in qualitative agreement with experimental results [3]. The situation is complicated by the fact that more recent theories for the single PE chain give different results, some confirming the simple scaling results described in Eqs. (18) and (21) [12, 21, 22], some confirming Eq. (18) while criticizing Eq. (21) [11, 23, 24]. This issue is not resolved and is under intense current investigation. For multivalent counterions, fluctuation effects can even give rise to a PE collapse purely due to electrostatic interactions [25–27], which is accompanied by a negative contribution to the effective persistence length [28].

2.7.3.1.1 **Manning Condensation** A peculiar phenomenon occurs for highly charged PEs and is known as the Manning

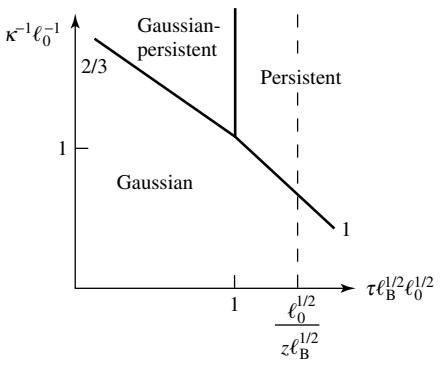

Fig. 5 Schematic phase diagram of a single semiflexible PE in bulk solution with bare persistence length ℓ_0 and line charge density τ, exhibiting various scaling regimes. High salt concentration and small τ correspond to the Gaussian regime, where the electrostatic interactions are irrelevant. In the persistent regime, the polymer persistence length is increased, and in the Gaussian-persistent regime, the polymer forms a persistent chain of Gaussian blobs as indicated in Fig. 4. The broken line indicates the Manning condensation, at which counterions condense on the polymer and reduce the effective polymer line charge density. We use a log–log plot, and the various power-law exponents for the crossover boundaries are denoted by numbers.

condensation of counterions [29, 30]. For a rigid PE represented by an infinitely long and straight cylinder with a linear charge density larger than

$$\ell_B \tau z = 1 \tag{23}$$

where z is the counterion valency, it was shown that counterions condense on the oppositely charged cylinder even in the limit of infinite solvent dilution. Real polymers have a finite length, and are neither completely straight nor in the infinite dilution limit [31, 32]. Still, Manning condensation has an experimental significance for polymer solutions because thermodynamic quantities, such as counterion activities [33] and osmotic coefficients [34], show a pronounced signature of Manning condensation. Locally, polymer segments can be considered as straight over length scales comparable to the persistence length. The Manning condition (Eq. 23) usually denotes a region where the binding of counterions to charged chain sections begins to deplete the solution from free counterions.

Within the scaling diagram of Fig. 5, the Manning threshold (denoted by a vertical broken line) is reached typically for charge densities larger than the one needed to straighten out the chain. This holds for monovalent ions provided $\ell_0 > \ell_B$, as is almost always the case. The Manning condensation of counterions will not have a profound influence on the local chain structure since the chain is rather straight already due to monomer–monomer repulsion. A more complete description of various scaling regimes related to Manning condensation, chain collapse, and chain swelling has recently been given [35, 36].

2.7.3.1.2 **Self-avoidance and Polyelectrolyte Chain Conformations** Let us now consider how the self-avoidance of PE chains comes into play, concentrating on the persistent regime defined by $\tau\sqrt{(\ell_B \ell_0)} > 1$. The end-to-end radius R of a strongly charged PE chain shows three distinct scaling ranges. For a chain length L smaller than the effective persistence length ℓ_{eff}, which according to Eq. (17) is the sum of the bare and electrostatic persistence lengths, R grows linearly with the length, $R \sim L$. Self-avoidance plays no role in this case because the chain is too short to fold back on itself.

For much longer chains, $L \gg \ell_{\text{eff}}$, we envision a single polymer coil as a solution of separate polymer pieces of length ℓ_{eff}, and treat their interactions using a virial expansion. The second-virial coefficient v_2 of a rod of length ℓ_{eff} and diameter d scales as $v_2 \sim \ell_{\text{eff}}^2 d$ [10]. The chain connectivity is taken into account by adding the entropic chain elasticity as a separate term. The standard Flory theory [7] for a semiflexible chain is based on writing the free energy $\mathcal{F}$ as a sum of two terms

$$\mathcal{F} \simeq \frac{R^2}{\ell_{\text{eff}} L} + v_2 R^3 \left(\frac{L/\ell_{\text{eff}}}{R^3}\right)^2 \tag{24}$$

where the first term is the entropic elastic energy associated with swelling a polymer chain to a radius R and the second term is the second-virial repulsive energy proportional to the coefficient v_2 and the segment density-squared. It is integrated over the volume R^3. The optimal radius R is calculated by minimizing this free energy and gives the swollen radius

$$R \sim \left(\frac{v_2}{\ell_{\text{eff}}}\right)^{1/5} L^{\nu} \tag{25}$$

with $\nu = 3/5$. This swollen radius is only realized above a minimal chain length $L > L_{\text{sw}} \sim \ell_{\text{eff}}^7 / v_2^2 \sim \ell_{\text{eff}}^3 / d^2$. For elongated segments with $\ell_{\text{eff}} \gg d$ or, equivalently, for a highly charged PE, we

obtain an intermediate range of chain lengths $\ell_{\text{eff}} < L < L_{\text{sw}}$ for which the chain is predicted to be Gaussian and the chain radius scales as

$$R \sim \ell_{\text{eff}}^{1/2} L^{1/2} \tag{26}$$

For charged chains, the effective rod diameter d is given in low salt concentrations by the screening length, that is, $d \sim \kappa^{-1}$ plus logarithmic corrections. The condition to have a Gaussian scaling range (Eq. 26) thus becomes $\ell_{\text{eff}} \gg \kappa^{-1}$. Within the persistent and the Gaussian-persistent scaling regimes depicted in Fig. 5, the effective persistence length is dominated by the electrostatic contribution and given by Eqs. (18) and (21), respectively, which in turn are always larger than the screening length κ^{-1}. It follows that a Gaussian scaling range (Eq. 26) always exists below the asymptotic swollen scaling range (Eq. 25). This situation is depicted in Fig. 4 for the Gaussian-persistent scaling regime, where the chain shows two distinct Gaussian scaling ranges at the small and large length scales. This multihierarchical scaling structure is only one of the many problems one faces when trying to understand the behavior of PE chains, be it experimentally, theoretically, or by simulations.

A different situation occurs when the polymer backbone is under bad-solvent conditions, in which case an intricate interplay between electrostatic chain swelling and short-range collapse occurs [37]. Quite recently, this interplay was theoretically shown to lead to a Rayleigh instability in the form of a necklace structure consisting of compact beads connected by thin strings [38–41]. Small-angle X-ray scattering on solvophobic PEs in a series of polar organic solvents of various solvent quality could qualitatively confirm these theoretical predictions [42].

2.7.3.2 Dilute Polyelectrolyte Solutions

It is natural to generalize the discussion of single-chain behavior to that of many PE chains at dilute concentrations. The dilute regime is defined by $c_{\text{m}} < c_{\text{m}}^*$, where c_{m} denotes the monomer concentration (per unit volume) and c_{m}^* is the concentration where individual chains start to overlap. Clearly, the overlap concentration is reached when the average bulk monomer concentration exceeds the monomer concentration inside a polymer coil. To estimate the overlap concentration c_{m}^*, we simply note that the average monomer concentration inside a coil with radius $R \simeq bN^{\nu}$ is given by

$$c_{\text{m}}^* \simeq \frac{N}{R^3} \simeq N^{1-3\nu} b^{-3} \tag{27}$$

For ideal chains with $\nu = 1/2$, the overlap concentration scales as $c_{\text{m}}^* \sim N^{-1/2}$ and thus decreases slowly as the polymerization index N increases. For rigid polymers with $\nu = 1$, the overlap concentration scales as $c_{\text{m}}^* \sim N^{-2}$ and decreases strongly as N increases. This means that the dilute regime for stiff PE chains corresponds to extremely low monomer concentrations. For example, taking a monomer size $b = 0.254\,\text{nm}$ and a polymerization index of $N = 10^4$, the overlap concentration becomes $c_{\text{m}}^* \approx 6 \times 10^{-7}\,\text{nm}^{-3} \approx 10^{-3}\,\text{mM}$, which is a very small concentration.

The osmotic pressure in the dilute regime in the limit $c_{\text{m}} \to 0$ is given by

$$\frac{\Pi}{k_{\text{B}}T} = \frac{f c_{\text{m}}}{z} + \frac{c_{\text{m}}}{N} \tag{28}$$

and consists of the ideal pressure of noninteracting counterions (first term) and polymer coils (second term). Note that since the second term scales as N^{-1}, it is quite small for large N and can be neglected. Hence, the main contribution to the osmotic pressure comes from the

counterion entropy. This entropic term explains also why charged polymers can be dissolved in water even when their backbone is quite hydrophobic. Precipitation of the PE chains will also mean that the counterions are confined within the precipitate. The entropy loss associated with this confinement is too large and keeps the polymers dispersed in solution. In contrast, for neutral polymers there are no counterions in solution. Only the second term in the osmotic pressure exists and contributes to the low osmotic pressure of these polymer solutions. In addition, this can explain the trend toward precipitation even for very small attractive interactions between neutral polymers.

2.7.3.3 Semidilute Polyelectrolyte Solution

In the semidilute concentration regime, $c_m > c_m^*$, different polymer coils are strongly overlapping, but the polymer solution is still far from being concentrated. This means that the volume fraction of the monomers in solution is much smaller than unity, $b^3 c_m \ll 1$. In this concentration range, the statistics of counterions and polymer fluctuations are intimately connected. One example in which this feature is particularly prominent is furnished by neutron and X-ray scattering from semidilute PE solutions [43–48].

The structure factor $S(q)$ shows a pronounced peak, which results from a competition between the connectivity of polymer chains and the electrostatic repulsion between charged monomers, as will be discussed below. An important length scale, schematically indicated in Fig. 6, is the mesh size or correlation length ξ, which measures the length below which entanglement effects between different chains are unimportant. The mesh size can be viewed as the polymer (blob) scale below which single-chain statistics are valid. A semidilute solution can be thought of being composed of roughly a close-packed array of polymer blobs of size ξ.

The starting point for the present discussion is the screened interaction between two charges immersed in a semidilute PE solution containing charged polymers, their counterions, and, possibly, additional salt ions. Screening in this case is produced not only by the ions but also by the charged chain segments that can be easily polarized and shield any free charges.

Using the random-phase approximation (RPA), the effective DH interaction can be written in Fourier space as [49, 50]

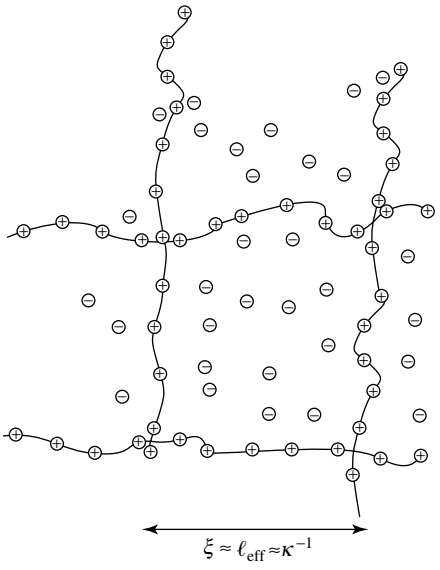

Fig. 6 Schematic view of the chain structure in the semidilute concentration range. The mesh size ξ is about equal to the effective polymer persistence length ℓ_{eff} and to the screening length κ^{-1} (if no salt is added to the system).

$$v_{\mathrm{RPA}}(q) = \frac{1 + v_2 c_{\mathrm{m}} S_0(q)}{c_{\mathrm{m}} f^2 S_0(q) + v_{\mathrm{DH}}^{-1}(q) + v_2 c_{\mathrm{m}} v_{\mathrm{DH}}^{-1}(q) S_0(q)} \tag{29}$$

recalling that c_{m} is the average density of monomers in solution and f is the fraction of charged monomers on each of the PE chains. The second-virial coefficient of monomer–monomer interactions is v_2 and the single-chain form factor (discussed below) is denoted by $S_0(q)$. In the case in which no chains are present, $c_{\mathrm{m}} = 0$, the RPA expression reduces to $v_{\mathrm{RPA}}(q) = v_{\mathrm{DH}}(q)$, the Fourier-transform of the DH potential of Eq. (9), given by

$$v_{\mathrm{DH}}(q) = \frac{4\pi \ell_{\mathrm{B}}}{q^2 + \kappa^2} \tag{30}$$

As before, κ^{-1} is the DH screening length, which is due to all mobile ions. We can write $\kappa^2 = \kappa_{\mathrm{salt}}^2 + 4\pi z \ell_{\mathrm{B}} f c_{\mathrm{m}}$, where $\kappa_{\mathrm{salt}}^2 = 8\pi z^2 \ell_{\mathrm{B}} c_{\mathrm{salt}}$ describes the screening due to added salt of valency $z:z$ and concentration c_{salt}, and the second term describes the screening due to the counterions of the PE monomers. Within the same RPA approximation, the monomer–monomer structure factor $S(q)$ of a polymer solution with monomer density c_{m} is given by [49, 50]

$$S^{-1}(q) = f^2 v_{\mathrm{DH}}(q) + \frac{S_0^{-1}(q)}{c_{\mathrm{m}}} + v_2 \tag{31}$$

The structure factor (or scattering function) only depends on the form factor of an isolated, noninteracting polymer chain, $S_0(q)$, the second-virial coefficient, v_2, the fraction f of charged monomers, and the interaction between monomers, which in the present case is taken to be the DH potential $v_{\mathrm{DH}}(q)$. The structure factor of a noninteracting semiflexible polymer is characterized, in addition to the monomer length b, by its persistence length ℓ_{eff}. In general, this form factor is a complicated function that cannot be written down in closed form [51, 52]. However, one can separate between three different ranges of wave numbers q, and within each range the form factor shows a rather simple scaling behavior, namely,

$$S_0^{-1}(q) \simeq \begin{cases} N^{-1} & \text{for} \quad q^2 < \dfrac{6}{Nb\ell_{\mathrm{eff}}} \\ \dfrac{q^2 b \ell_{\mathrm{eff}}}{6} & \text{for} \quad \dfrac{6}{Nb\ell_{\mathrm{eff}}} < q^2 < \dfrac{36}{\pi^2 \ell_{\mathrm{eff}}^2} \\ \dfrac{qb}{\pi} & \text{for} \quad \dfrac{36}{\pi^2 \ell_{\mathrm{eff}}^2} < q^2 \end{cases} \tag{32}$$

For small wave numbers the polymer acts like a point scatterer, while in the intermediate wave number regime the polymer behaves like a flexible, Gaussian polymer, and for the largest wave numbers the polymer can be viewed as a stiff rod.

One of the most interesting features of semidilute PE solutions is the fact that the structure factor $S(q)$ shows a pronounced peak. For weakly charged PEs, the peak position scales as $q \sim c_{\mathrm{m}}^{1/4}$ with the monomer density [45], in agreement with the aforementioned RPA results for charged polymers [49, 50]. We now discuss the scaling of the characteristic scattering peak within the present formalism. The position of the peak follows from the inverse structure factor (Eq. 31), via $\partial S^{-1}(q)/\partial q = 0$, which leads to the equation

$$q^2 + \kappa_{\mathrm{salt}}^2 + 4\pi z \ell_{\mathrm{B}} f c_{\mathrm{m}} = \left(\frac{8\pi q \ell_{\mathrm{B}} f^2 c_{\mathrm{m}}}{\partial S_0^{-1}(q)/\partial q} \right)^{1/2} \tag{33}$$

In principle, there are two distinct scaling behaviors possible for the peak, depending

on whether the chain form factor of Eq. (32) exhibits flexible-like or rigid-like scaling. Concentrating now on the flexible case, that is, the intermediate q-range in Eq. (32), the peak of $S(q)$ scales as

$$q^* \simeq \left(\frac{24\pi \ell_B f^2 c_m}{b \ell_{eff}} \right)^{1/4} \qquad (34)$$

in agreement with experimental results. A peak is only obtained if the left-hand side of Eq. (33) is dominated by the q-dependent part, that is, if $(q^*)^2 > \kappa_{salt}^2 + 4\pi z \ell_B f c_m$.

In Fig. 7(a) we show density-normalized scattering curves for a PE solution characterized by the persistence length $\ell_{eff} = 1$ nm (taken to be constant and thus independent of the monomer concentration), with monomer length $b = 0.38$ nm (as appropriate for poly-DADMAC) and charge fraction $f = 0.5$ and with no added salt. As the monomer density decreases (bottom to top in the figure), the peak moves to smaller wave numbers and sharpens, in agreement with previous implementations of the RPA. In Fig. 7(b) we show the same data in a different representation. Here we clearly demonstrate that the large-q region already is dominated by the $1/q$ behavior of the single-chain structure factor, $S_0(q)$. Since neutron-scattering data easily extend to wave numbers as high as $q \sim 5\,\mathrm{nm}^{-1}$, the stiff rodlike behavior in the high q-limit, exhibited on such a plot, will be important in interpreting and fitting experimental data even at lower q-values.

In a semidilute solution there are three different, and in principle, independent length scales: the mesh size ξ, the

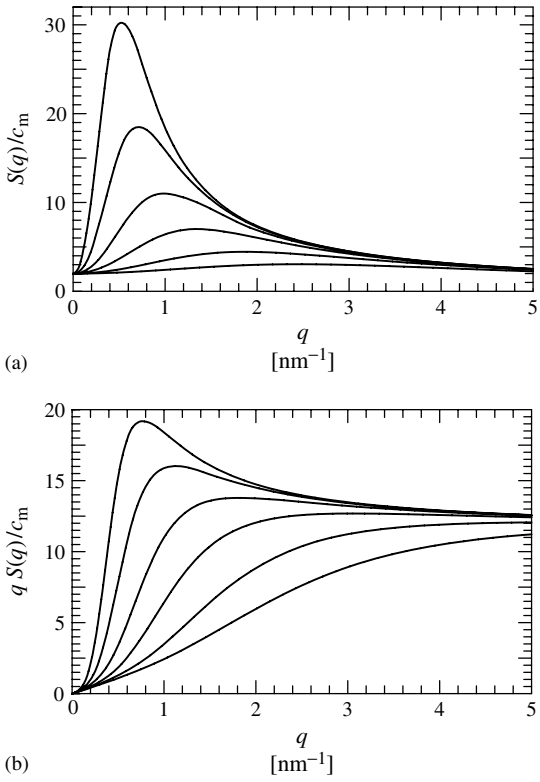

Fig. 7 (a) RPA prediction for the rescaled structure factor $S(q)/c_m$ of a semidilute PE solution with persistence length $\ell_{eff} = 1$ nm, monomer length $b = 0.38$ nm, and charge fraction $f = 0.5$ in the salt-free case. The monomer densities are (from bottom to top) $c_m = 1$ M, 0.3 M, 10 mM, 3 mM, 1 mM, and 0.3 mM. (b) For the same series of c_m values as in (a), the structure factor is multiplied by the wave number q. The semiflexibility becomes more apparent because for large q the curves tend toward a constant.

screening length κ^{-1}, and the persistence length ℓ_{eff}. In the absence of added salt, the screening length scales as

$$\kappa^{-1} \sim (z\ell_{\text{B}} f c_{\text{m}})^{-1/2} \tag{35}$$

Assuming that the persistence length is larger or of the same order of magnitude as the mesh size, as is depicted in Fig. 6, the polymer chains can be thought of straight segments between different crossing links. Denoting the number of monomers inside a correlation blob as g, this means that $\xi \sim bg$. The average monomer concentration scales as $c_{\text{m}} \sim g/\xi^3$, from which we conclude that

$$\xi \sim (bc_{\text{m}})^{-1/2} \tag{36}$$

Finally, the persistence length within a semidilute PE solution can be calculated by considering the electrostatic energy cost for slightly bending a charged rod. In PE solutions, it is important to include in addition to the screening by salt ions the screening due to charged chain segments. This can be calculated by using the RPA interaction (Eq. 29). Since the screening due to polymer chains is scale-dependent and increases for large separations, a q-dependent instability is encountered and leads to a persistence length [53]

$$\ell_{\text{OSF}}^{\text{sd}} \sim (bc_{\text{m}})^{-1/2} \tag{37}$$

where the ''sd'' superscript stands for ''semidilute.'' This result is a generalization of the OSF result for a single chain and applies to semidilute solutions. Comparing the three lengths, we see that

$$\xi \sim \ell_{\text{OSF}}^{\text{sd}} \sim \sqrt{\frac{z\ell_{\text{B}} f}{b}}\kappa^{-1} \tag{38}$$

Since the prefactor $\sqrt{(\ell_{\text{B}} f/b)}$ for synthetic fully charged polymers is roughly of order unity, one finds that for salt-free semidilute PE solutions, all three length-scales scale in the same manner with c_{m}, namely, as $\sim c_{\text{m}}^{-1/2}$, as is known also from experiments [43, 44, 54] and previous theoretical calculations [55, 56]. In simulations of many PE chains, the reduction of the chain size due to screening by PE chains was clearly seen [57–60].

2.7.4 Adsorption of a Single Polyelectrolyte Chain

After reviewing bulk properties of PE solutions, we elaborate on the adsorption diagram of a single semiflexible PE on an oppositely charged substrate. In contrast to the adsorption of neutral polymers, the resulting phase diagram shows a large region where the adsorbed polymer is flattened out on the substrate and creates a dense adsorption layer.

Experimentally, the adsorption of charged polymers on charged or neutral substrates has been characterized as a function of the polymer charge, chemical composition of the substrate, pH, and ionic strength of the solution [61, 62], as well as the substrate charge density [63–68]. Repeated adsorption of anionic and cationic PEs can lead to well-characterized multilayers on planar [69–74] and spherical substrates [75–77]. Theoretically, the adsorption of PEs on charged surfaces poses a much more complicated problem than the corresponding adsorption of neutral polymers. The adsorption process results from a subtle balance between electrostatic repulsion between charged monomers, leading to chain stiffening, and electrostatic attraction between the substrate and the polymer chain. The adsorption problem has been treated theoretically employing the uniform expansion method [78] and various continuous mean-field theories [79–83]. In all these

works, the polymer density is taken to be constant in directions parallel to the surface.

The adsorption of a single semiflexible and charged chain on an oppositely charged plane [84] can be treated as a generalization of the adsorption of flexible polymers [85]. A PE characterized by the linear charge density τ is subject to an electrostatic potential created by σ, the homogeneous surface charge density (per unit area). Because this potential is attractive for an oppositely charged substrate, we consider it as the driving force for the adsorption. More complex interactions are neglected. They are due to the dielectric discontinuity at the substrate surface and are due to the impenetrability of the substrate for salt ions.

An ion in solution has a repulsive interaction from the surface when the solution dielectric constant is higher than that of the substrate. This effect can lead to desorption for highly charged PE chains. On the contrary, when the substrate is a metal, there is a possibility to induce PE adsorption on noncharged substrates or on substrates bearing charges of the same sign as the PE. See Ref. [84] for more details.

Within the linearized DH theory, the electrostatic potential of a homogeneously charged plane is

$$V_{\text{plane}}(x) = 4\pi \ell_{\text{B}} \sigma \kappa^{-1} \text{e}^{-\kappa x} \qquad (39)$$

Assuming that the polymer is adsorbed over a layer of width δ smaller than the screening length κ^{-1}, the electrostatic attraction force per monomer unit length can be written as

$$f_{\text{att}} = -4\pi \ell_{\text{B}} \sigma \tau \qquad (40)$$

We neglect nonlinear effects due to counterion condensation. They are described by the Gouy-Chapman (GC) theory for counterion distribution close to a charged surface. Although these effects are clearly important, it is difficult to include them systematically, and we remain at the linearized DH level.

Because of the confinement in the adsorbed layer, the polymer feels an entropic repulsion. If the layer thickness δ is much smaller than the effective persistence length of the polymer, ℓ_{eff}, as depicted in Fig. 8(a), a new length scale, the so-called deflection length λ, enters the description of the polymer statistics. The deflection length λ measures the average distance between two contact points of the polymer chain with the substrate. As shown by Odijk, the deflection length scales as $\lambda \sim \delta^{2/3} \ell_{\text{eff}}^{1/3}$ and is larger than the layer thickness δ but smaller than the persistence length ℓ_{eff} [86, 87]. The entropic repulsion follows in a simple manner from the deflection length by assuming that the polymer loses roughly a free energy of one $k_{\text{B}}T$ per deflection length.

On the other hand, if $\delta > \ell_{\text{eff}}$, as shown in Fig. 8(b), the polymer forms a random coil with many loops within the adsorbed layer. For a contour length smaller than $L \sim \delta^2/\ell_{\text{eff}}$, the polymer obeys Gaussian statistics and decorrelates into blobs with an entropic cost of one $k_{\text{B}}T$ per blob. The entropic repulsion force per monomer unit length is thus [86, 87]

$$f_{\text{rep}} \sim \begin{cases} \delta^{-5/3} \ell_{\text{eff}}^{-1/3} & \text{for} \quad \delta \ll \ell_{\text{eff}} \\ \ell_{\text{eff}} \delta^{-3} & \text{for} \quad \delta \gg \ell_{\text{eff}} \end{cases} \qquad (41)$$

where we neglected a logarithmic correction factor that is not important for the scaling arguments. As shown in the preceding section, the effective persistence length ℓ_{eff} depends on the screening length and the line charge density; in

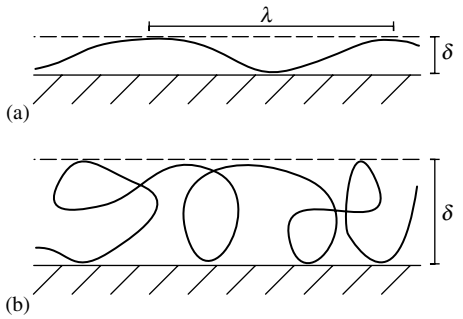

Fig. 8 (a) Schematic picture of the adsorbed polymer layer when the effective persistence length is larger than the layer thickness, $\ell_{\text{eff}} > \delta$. The distance between two contacts of the polymer with the substrate, the so-called deflection length, scales as $\lambda \sim \delta^{2/3}\ell_{\text{eff}}^{1/3}$. (b) Adsorbed layer for the case when the persistence length is smaller than the layer thickness, $\ell_{\text{eff}} < \delta$. In this case the polymer forms a random coil with many loops and a description in terms of a flexible polymer model becomes appropriate.

essence, one has to keep in mind that ℓ_{eff} is larger than ℓ_0 for a wide range of parameters because of electrostatic stiffening effects.

The situation is complicated by the fact that the electrostatic contribution to the persistence length is scale-dependent and decreases as the chain is bent at length scales smaller than the screening length. This leads to modifications of the entropic confinement force (Eq. 41) if the deflection length is smaller than the screening length. As can be checked explicitly, all results reported here are not changed by these modifications.

The equilibrium layer thickness follows from equating the attractive and repulsive forces (Eqs. 40 and 41). For rather stiff polymers and small layer thickness, $\delta < \kappa^{-1} < \ell_{\text{eff}}$, we obtain

$$\delta \sim (\ell_{\text{B}}\sigma\tau\ell_{\text{eff}}^{1/3})^{-3/5} \tag{42}$$

For a layer thickness corresponding to the screening length, $\delta \approx \kappa^{-1}$, scaling arguments predict a rather abrupt desorption transition [84]. This is in accord with previous transfer-matrix calculations for a semiflexible polymer bound by short-ranged (square-well) potentials [88–91]. Setting $\delta \sim \kappa^{-1}$ in Eq. (42), we obtain an expression for the adsorption threshold (for $\kappa\ell_{\text{eff}} > 1$)

$$\sigma^* \sim \frac{\kappa^{5/3}}{\tau\ell_{\text{B}}\ell_{\text{eff}}^{1/3}} \tag{43}$$

For $\sigma > \sigma^*$, the polymer is adsorbed and localized over a layer with a width smaller than the screening length (and with the condition $\ell_{\text{eff}} > \kappa^{-1}$ also satisfying $\delta < \ell_{\text{eff}}$). As σ is decreased, the polymer abruptly desorbs at the threshold $\sigma = \sigma^*$. In the Gaussian regime, the effective persistence length ℓ_{eff} is given by the bare persistence length ℓ_0 and the desorption threshold is obtained by replacing ℓ_{eff} by ℓ_0 in Eq. (43), that is,

$$\sigma^* \sim \frac{\kappa^{5/3}}{\tau\ell_{\text{B}}\ell_0^{1/3}} \tag{44}$$

In the persistent regime, we have $\ell_{\text{eff}} \sim \ell_{\text{OSF}}$ with ℓ_{OSF} given by Eq. (18). The adsorption threshold follows from Eq. (43) as

$$\sigma^* \sim \frac{\kappa^{7/3}}{\tau^{5/3}\ell_{\text{B}}^{4/3}} \tag{45}$$

Finally, in the Gaussian-persistent regime, we have an effective line charge density from Eq. (20) and a modified persistence length (Eq. 21). For the adsorption threshold, we obtain from Eq. (43)

$$\sigma^* \sim \frac{\kappa^{7/3}\ell_0^{5/9}}{\tau^{5/9}\ell_B^{7/9}} \tag{46}$$

Let us now consider the opposite limit, $\ell_{eff} < \kappa^{-1}$. From Eq. (42), we see that the layer thickness δ is of the same order as ℓ_{eff} for $\ell_B \sigma \tau \ell_{eff}^2 \sim 1$, at which point the condition $\delta \ll \ell_{eff}$ used in deriving Eq. (42) breaks down. If the layer thickness is larger than the persistence length but smaller than the screening length, $\ell_{eff} < \delta < \kappa^{-1}$, the prediction for δ obtained from balancing Eqs. (40) and (41) becomes

$$\delta \sim \left(\frac{\ell_{eff}}{\ell_B \sigma \tau}\right)^{1/3} \tag{47}$$

From this expression we see that δ has the same size as the screening length κ^{-1} for

$$\sigma^* \sim \frac{\ell_{eff}\kappa^3}{\tau \ell_B} \tag{48}$$

This in fact denotes the location of a continuous adsorption transition at which the layer grows to infinity. The scaling results for the adsorption behavior of a flexible polymer (Eqs. 47–48) are in agreement with previous results [78].

In Fig. 9 we show the desorption transitions and the line at which the adsorbed layer crosses over from being flat, $\delta < \ell_{eff}$, to being crumpled or coiled, $\delta > \ell_{eff}$. The underlying PE behavior in the bulk, as shown in Fig. 5, is denoted by broken lines. We obtain two different phase diagrams, depending on the value of the parameter

$$\Sigma = \sigma \ell_0^{3/2} \ell_B^{1/2} \tag{49}$$

For strongly charged surfaces, $\Sigma > 1$, we obtain the phase diagram as in Fig. 9(a), and for weakly charged surfaces, $\Sigma < 1$, as in Fig. 9(b). We see that strongly charged PEs, obeying $\tau\sqrt{(\ell_0 \ell_B)} > 1$, always adsorb in flat layers. The scaling of the desorption transitions is in general agreement with recent computer simulations of charged PEs [92].

2.7.4.1 Adsorption on Curved Substrates

Adsorption of PEs on curved substrates is of importance because PEs are

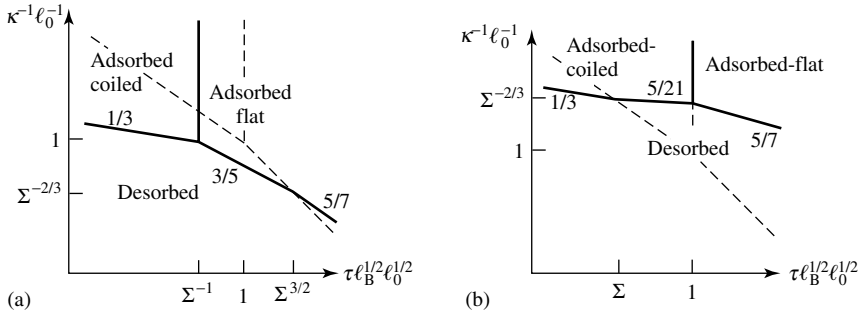

Fig. 9 Adsorption scaling diagram shown on a log–log plot for (a) strongly charged surfaces, $\Sigma = \sigma \ell_0^{3/2} \ell_B^{1/2} > 1$, and for (b) weakly charged surfaces, $\Sigma < 1$. We find a desorbed regime, an adsorbed phase in which the polymer is flat and dense, and an adsorbed phase in which the polymer shows loops. It is seen that a fully charged PE is expected to adsorb in a flat layer, whereas charge-diluted PEs can form coiled layers with loops and dangling ends. The broken lines denote the scaling boundaries of PE chains in the bulk as shown in Fig. 5. The numbers on the lines indicate the power-law exponents of the crossover boundaries between the regimes.

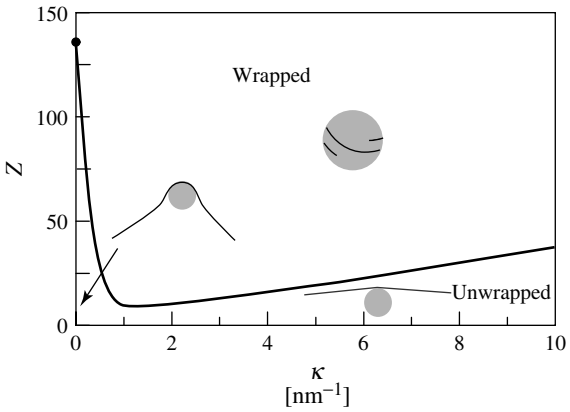

Fig. 10 Numerically determined adsorption diagram for a charged semiflexible polymer of length $L = 50\,\text{nm}$, linear charge density $\tau = 6\,\text{nm}^{-1}$, persistence length $\ell_0 = 30\,\text{nm}$, interacting with an oppositely charged sphere of radius $R_p = 5\,\text{nm}$. Shown is the main transition from the unwrapped configuration (at the bottom) to the wrapped configuration (at the top) as a function of sphere charge Z and inverse screening length κ. Wrapping is favored at intermediate salt concentrations. The parameters are chosen for the problem of DNA-histone complexation. (Adapted from Ref. [99].)

widely used to stabilize colloidal suspensions [93] and to fabricate hollow polymeric shells [75–77]. When the curvature of the small colloidal particles is large enough, it can lead to a much more pronounced effect for PE adsorption as compared with neutral polymer. This is mainly due to the fact that the electrostatic energy of the adsorbed PE layer depends sensitively on curvature [94–98]. Bending a charged polymer around a small sphere costs a large amount of electrostatic energy, which will disfavor adsorption of long, strongly charged PE at very low salt concentrations.

In Fig. 10 we show the adsorption phase diagram of a single stiff PE of finite length that interacts with an oppositely charged sphere of charge Z (in units of e). The specific parameters were chosen as appropriate for the complexation of DNA (a negatively charged, relatively stiff biopolymer) with positively charged histone proteins, corresponding to a DNA length of $L = 50\,\text{nm}$, a chain persistence length of $\ell_0 = 30\,\text{nm}$, and a sphere radius of $R_p = 5\,\text{nm}$. The phase diagram was obtained by minimization of the total energy including bending energy of the DNA, electrostatic attraction between the sphere and the DNA, and electrostatic repulsion between the DNA segments with respect to the chain configuration [99]. Configurational fluctuations away from this ground state are unimportant for such stiff polymers.

We show in Fig. 10 the main transition between an unwrapped state, at low sphere charge Z, and the wrapped state, at large sphere charge Z. It is seen that at values of the sphere charge between $Z = 10$ and $Z = 130$, the wrapping only occurs at intermediate values of the inverse screening length $\kappa \sim c_{\text{salt}}^{1/2}$. At low salt concentrations (lower left corner in the phase diagram), the self-repulsion between DNA segments prevents wrapping, while at large salt concentrations (lower right corner in the diagram), the electrostatic attraction is not strong enough to overcome the mechanical bending energy of the DNA molecule. These results are in good agreement with experiments on DNA/histone complexes [100]. Interestingly, the optimal salt concentration, where a minimal sphere charge is needed to wrap the DNA, occurs at physiological salt concentration, for $\kappa^{-1} \approx 1\,\text{nm}$. For colloidal particles of larger size and for flexible synthetic

polymers, configurational fluctuations become important. They have been treated using a mean-field description in terms of the average monomer density profile around the sphere [101, 102].

2.7.5 Adsorption from Semidilute Solutions

So far we have been reviewing the behavior of single PE chains close to a charged wall (or surface). This will now be extended to include adsorption of PEs from bulk (semidilute) solutions having a bulk concentration c_m^b. As before, the chains are assumed to have a fraction f of charged monomers, each carrying a charge e, resulting in a linear charge density $\tau = f/b$ on the chain. The solution can also contain salt (small ions) of concentration c_{salt}, which is directly related to the DH screening length, κ^{-1}. For clarity purposes, the salt is assumed to be monovalent ($z = 1$) throughout Sect. 2.7.5.

We will consider adsorption only onto a single flat and charged surface. Clearly, the most important quantity is the profile of the polymer concentration $c_m(x)$ as function of x, the distance from the wall. Another useful quantity is the polymer surface excess per unit area, defined as

$$\Gamma = \int_0^\infty [c_m(x) - c_m^b]\,dx \qquad (50)$$

Related to the surface excess Γ is the amount of charges (in units of e) carried by the adsorbing PE chains, $f\Gamma$. In some cases the polymer carries a higher charge (per unit area) than the charged surface itself, $f\Gamma > \sigma$, and the surface charge is overcompensated by the PE, as we will see later. This does not violate charge neutrality in the system because of the presence of counterions in solution.

In many experiments, the total amount of polymer surface excess Γ is measured as a function of the bulk polymer concentration, pH, and/or ionic strength of the bulk solution [103–110]. For reviews see, for example, Refs. [61, 62, 111, 112]. More recently, spectroscopy [105] and ellipsometry [109] have been used to measure the width of the adsorbed PE layer. Other techniques such as neutron-scattering can be employed to measure the entire profile $c_m(x)$ of the adsorbed layer [113, 114].

In spite of the difficulties in treating theoretically PEs in solution because of the delicate interplay between the chain connectivity and the long range nature of electrostatic interactions [1, 9, 115, 116], several simple approaches treating adsorption exist.

One approach is a discrete *multi-Stern layer* model [117–121], where the system is placed on a lattice whose sites can be occupied by a monomer, a solvent molecule, or a small ion. The electrostatic potential is determined self-consistently (mean-field approximation) together with concentration profiles of the polymer and small ions.

In another approach, the electrostatic potential and the PE concentration are treated as continuous functions [78, 80–82, 122–125]. These quantities are obtained from two coupled differential equations derived from the total free energy of the system. We will review the main results of the latter approach, presenting numerical solutions and scaling arguments of the mean-field profiles.

2.7.5.1 Mean-field Theory and its Profile Equations

The charge density on the polymer chains is assumed to be continuous and uniformly distributed along the chains.

Further treatments of the polymer charge distribution (annealed and quenched models) can be found in Refs. [81, 82, 123].

Within mean-field approximation, the free energy of the system can be expressed in terms of the local electrostatic potential $\psi(\mathbf{r})$, the local monomer concentration $c_{\mathrm{m}}(\mathbf{r})$, and the local concentration of positive and negative ions $c^{\pm}(\mathbf{r})$. The mean-field approximation means that the influence of the charged surface and the interchain interactions can be expressed in terms of an external potential that will determine the local concentration of the monomers, $c_{\mathrm{m}}(\mathbf{r})$. This external potential depends both on the electrostatic potential and on the excluded volume interactions between the monomers and the solvent molecules. The excess free energy with respect to the bulk can then be calculated using another important approximation, the ground state dominance. This approximation is used often for neutral polymers [9] and is valid for very long polymer chains, $N \gg 1$. It is then convenient to introduce the polymer order parameter $\phi(\mathbf{r})$, where $c_{\mathrm{m}}(\mathbf{r}) = |\phi(\mathbf{r})|^2$, and to express the adsorption free energy $\mathcal{F}$ in terms of ϕ and ψ (and in units of $k_{\mathrm{B}}T$) [80–82, 122–124]

$$\mathcal{F} = \int \mathrm{d}\mathbf{r}\{F_{\mathrm{pol}}(\mathbf{r}) + F_{\mathrm{ions}}(\mathbf{r}) + F_{\mathrm{el}}(\mathbf{r})\} \tag{51}$$

The polymer contribution is

$$F_{\mathrm{pol}}(\mathbf{r}) = \frac{a^2}{6}|\nabla\phi|^2 + \frac{1}{2}v_2(\phi^4 - \phi_b^4) - \mu_p(\phi^2 - \phi_b^2) \tag{52}$$

where the first term is the polymer elastic energy. Throughout this section we restrict ourselves to flexible chains and treat the Kuhn length a and the effective monomer size b as the same parameter. The second term is the excluded volume contribution where the second-virial coefficient v_2 is of order a^3. The last term couples the system to a polymer reservoir via a chemical potential μ_p, and $\phi_b = \sqrt{c_{\mathrm{m}}^b}$ is related to the bulk monomer concentration, c_{m}^b.

The entropic contribution of the small (monovalent) ions is

$$F_{\mathrm{ions}}(\mathbf{r}) = \sum_{i=\pm}[c^i \ln c^i - c^i - c_{\mathrm{salt}} \ln c_{\mathrm{salt}} + c_{\mathrm{salt}}] - \mu^i(c^i - c_{\mathrm{salt}}) \tag{53}$$

where $c^i(\mathbf{r})$ and μ^i are, respectively, the local concentration and the chemical potential of the $i = \pm$ ions, while c_{salt} is the bulk concentration of salt.

Finally, the electrostatic contributions (per $k_{\mathrm{B}}T$) are

$$F_{\mathrm{el}}(\mathbf{r}) = \frac{\left[f e\phi^2\psi + ec^+\psi - ec^-\psi - \frac{\varepsilon}{8\pi}|\nabla\psi|^2\right]}{k_{\mathrm{B}}T} \tag{54}$$

The first three terms are the electrostatic energies of the monomers, the positive ions, and the negative ions, respectively; f is the fractional charge carried by one monomer. The last term is the self-energy of the electric field where ε is the dielectric constant of the solution. Note that the electrostatic contribution (Eq. 54) is equivalent to the well-known result: $(\varepsilon/8\pi k_{\mathrm{B}}T)\int \mathrm{d}\mathbf{r}|\nabla\psi|^2$ plus surface terms. This can be seen by substituting the Poisson–Boltzmann equation (as obtained below) into Eq. (54) and then integrating by parts.

Minimization of the free energy (Eqs. 51–54) with respect to $c^{\pm}$, ϕ, and ψ yields a Boltzmann distribution for the density of the small ions, $c^{\pm}(\mathbf{r}) = c_{\mathrm{salt}} \exp(\mp e\psi/k_{\mathrm{B}}T)$, and two coupled differential equations for ϕ and ψ:

$$\nabla^2\psi(\mathbf{r}) = \frac{8\pi e}{\varepsilon} c_{\text{salt}} \sinh\left(\frac{e\psi}{k_B T}\right) - \frac{4\pi e}{\varepsilon}(f\phi^2 - f\phi_b^2 e^{e\psi/k_B T}) \tag{55}$$

$$\frac{a^2}{6}\nabla^2\phi(\mathbf{r}) = v_2(\phi^3 - \phi_b^2\phi) + \frac{f\phi e\psi}{k_B T} \tag{56}$$

Equation (55) is a generalized Poisson–Boltzmann equation including the free ions and the charged polymers. The first term represents the salt contribution and the second term is due to the charged monomers and their counterions. Equation (56) is a generalization of the self-consistent field equation of neutral polymers [9]. In the bulk, the above equations are satisfied by setting $\psi \to 0$ and $\phi \to \phi_b$.

2.7.5.2 Numerical Profiles: Constant ψ_s

When the surface is taken as ideal, that is, flat and homogeneous, the physical quantities depend only on the distance x from the surface. The surface imposes boundary conditions on the polymer order parameter $\phi(x)$ and electrostatic potential $\psi(x)$. In thermodynamic equilibrium, all charge carriers in solution should exactly balance the surface charges (charge neutrality). The Poisson–Boltzmann Equation (55), the self-consistent field Equation (56), and the boundary conditions uniquely determine the polymer concentration profile and the electrostatic potential. In most cases, these two coupled nonlinear equations can only be solved numerically.

We present now numerical profiles obtained for surfaces with a constant potential ψ_s:

$$\psi|_{x=0} = \psi_s \tag{57}$$

The boundary conditions for $\phi(x)$ depend on the nature of the short-range nonelectrostatic interactions of the monomers and the surface. For simplicity, we take a nonadsorbing surface and require that the monomer concentration will vanish there:

$$\phi|_{x=0} = 0 \tag{58}$$

We note that the boundary conditions chosen in Eqs. (57) to (58) model the particular situation of electrostatic attraction in competition with a short-range (steric) repulsion of nonelectrostatic origin. Possible variations of these boundary conditions include surfaces with a constant surface charge (discussed later) and surfaces with a nonelectrostatic short-range attractive (or repulsive) interaction with the polymer [83, 127]. Far from the surface ($x \to \infty$), both ψ and ϕ reach their bulk values and their derivatives vanish: $\psi'|_{x\to\infty} = 0$ and $\phi'|_{x\to\infty} = 0$.

The numerical solutions of the mean-field Eqs. (55) and (56) together with the boundary conditions discussed above are presented in Fig. 11, for several different physical parameters.

The polymer is positively charged and is attracted to the nonadsorbing surface held at a constant negative potential. The aqueous solution contains a small amount of monovalent salt ($c_{\text{salt}} = 0.1\,\text{mM}$). The reduced concentration profile $c_m(x)/\phi_b^2$ is plotted as a function of the distance from the surface x. Different curves correspond to different values of the reduced surface potential $y_s \equiv e\psi_s/k_B T$, the charge fraction f, and the effective monomer size a.

Although the spatial variation of the profiles differs in detail, they all have a single peak that can be characterized by its height and width. This observation

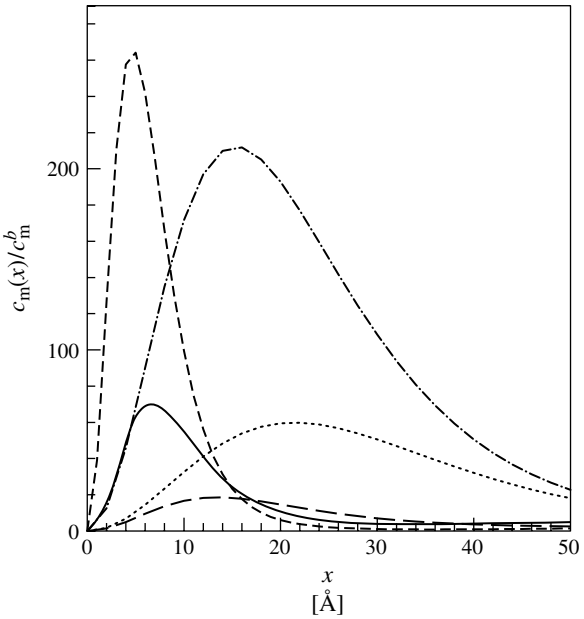

Fig. 11 Adsorption profiles obtained by numerical solutions of Eqs. (55) and (56) for several sets of physical parameters in the low-salt limit. The polymer concentration scaled by its bulk value $c_m^b = \phi_b^2$ is plotted as a function of the distance from the surface. The different curves correspond to: $f = 1$, $a = 5$ Å and $\gamma_s = e\psi_s/k_BT = -0.5$ (solid curve); $f = 0.1$, $a = 5$ Å and $\gamma_s = -0.5$ (dots); $f = 1$, $a = 5$ Å and $\gamma_s = -1.0$ (short dashes); $f = 1$, $a = 10$ Å and $\gamma_s = -0.5$ (long dashes); and $f = 0.1$, $a = 5$ Å and $\gamma_s = 1.0$ (dot–dash line). For all cases, $\phi_b^2 = 10^{-6}$ Å^{-3}, $\nu_2 = 50$ Å^3, $\varepsilon = 80$, $T = 300$ K, and $c_{salt} = 0.1$ mM. (Adapted from Ref. [124].)

serves as a motivation to using scaling arguments.

2.7.5.3 Scaling Results

The numerical profiles of the previous section indicate that it may be possible to obtain simple analytical results for the PE adsorption by assuming that the adsorption is characterized by one dominant length scale D. Hence, we write the polymer order parameter profile in the form

$$\phi(x) = \sqrt{c_M}\, h(x/D) \qquad (59)$$

where $h(x)$ is a dimensionless function normalized to unity at its maximum and c_M sets the scale of polymer adsorption, such that $\phi(D) = \sqrt{c_M}$. The free energy can now be expressed in terms of D and c_M, while the exact form of $h(x)$ affects only the numerical prefactors.

In principle, the adsorption length D depends also on the ionic strength through κ^{-1}. As discussed below, the scaling assumption (Eq. 59) is only valid as long as κ^{-1} and D are not of the same order of magnitude. Otherwise, h should be a function of both κx

and x/D. We concentrate now on two limiting regimes where Eq. (59) can be justified: (1) the low-salt regime $D \ll \kappa^{-1}$ and (2) the high-salt regime $D \gg \kappa^{-1}$. We first discuss the case of constant surface potential, which can be directly compared to the numerical profiles. Then we note the differences with the constant surface charge boundary condition in which the interesting phenomenon of charge overcompensation is discussed in detail.

2.7.5.3.1 **Low-salt Regime $D \ll \kappa^{-1}$ and ψ_s = constant** In the low-salt regime the effect of the small ions can be neglected and the free energy (per unit surface area) (Eqs. 51–54) is approximated by (see also Refs. [80, 124])

$$F \simeq \frac{a^2}{6D} c_M - f|y_s| c_M D + 4\pi l_B f^2 c_M^2 D^3 + \frac{1}{2} v_2 c_M^2 D \quad (60)$$

In the above equation and in what follows, we neglect additional prefactors of order unity in front of the various terms that arise from inserting the scaling profile (Eq.59) into the free energy. The first term of Eq. (60) is the elastic energy characterizing the response of the polymer to concentration inhomogeneities. The second term accounts for the electrostatic attraction of the polymers to the charged surface. The third term represents the Coulomb repulsion between adsorbed monomers. The last term represents the excluded volume repulsion between adsorbed monomers, where we assume that the monomer concentration near the surface is much larger than the bulk concentration $c_M \gg \phi_b^2$.

In the low-salt regime and for highly charged PEs, the electrostatic interactions are much stronger than the excluded volume ones.

Neglecting the latter interactions and minimizing the free energy with respect to D and c_M gives

$$D^2 \simeq \frac{a^2}{f|y_s|} \sim \frac{1}{f|\psi_s|} \quad (61)$$

and

$$c_M \simeq \frac{|y_s|^2}{4\pi l_B a^2} \sim |\psi_s|^2 \quad (62)$$

recalling that $y_s = e\psi_s/k_B T$. As discussed above, these expressions are valid as long as (1) $D \ll \kappa^{-1}$ and (2) the excluded volume term in Eq. (60) is negligible. Condition (1) translates into $c_{salt} \ll f|y_s|/(8\pi l_B a^2)$. For $|y_s| \simeq 1$, $a = 5$ Å and $l_B = 7$ Å this limits the salt concentration to $c_{salt}/f \ll 0.4$ M. Condition (2) on the magnitude of the excluded volume term can be shown to be equivalent to $f \gg v_2|y_s|/l_B a^2$. These requirements are consistent with the data presented in Fig. 11.

We recall that the profiles presented in Fig. 11 were obtained from the numerical solution of Eqs. (55) and (56), including the effect of small ions and excluded volume. The scaling relations are verified by plotting in Fig. 12 the same sets of data as in Fig. 11, using rescaled variables as defined in Eqs. (61) and (62). That is, the rescaled electrostatic potential $\psi(x)/\psi_s$ and polymer concentration $c_m(x)/c_M \sim c_m(x)a^2/|y_s|^2$ are plotted as functions of the rescaled distance $x/D \sim x f^{1/2}|y_s|^{1/2}/a$. The different curves roughly collapse on the same curve.

In many experiments the total amount of adsorbed polymer per unit area Γ is measured as function of the physical characteristics of the system such as the charge fraction f, the pH of the solution, or the salt concentration c_{salt} [103–110].

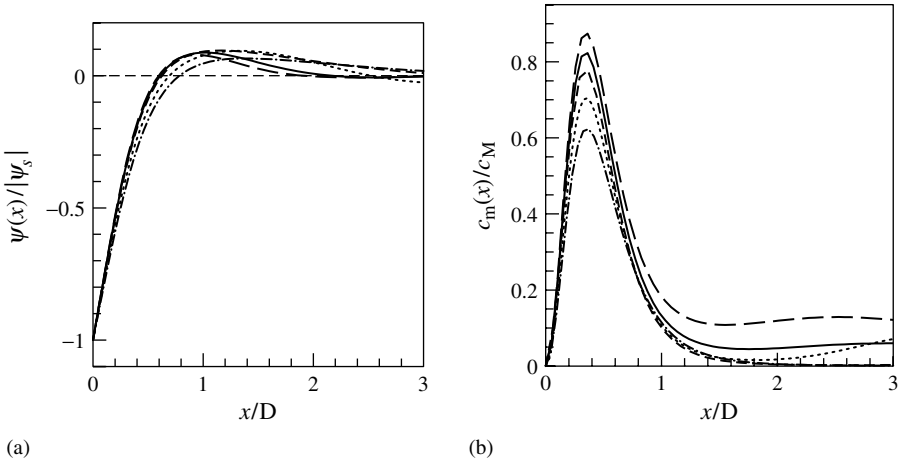

Fig. 12 Scaling behavior of PE adsorption in the low-salt regime (Eqs. 61 and 62). (a) The rescaled electrostatic potential $\psi(x)/|\psi_s|$ as a function of the rescaled distance x/D. (b) The rescaled polymer concentration $c_m(x)/c_M$ as a function of the same rescaled distance. The profiles are taken from Fig. 11 (with the same notation). (Adapted from Ref. [124].)

This quantity can be easily obtained from our scaling expressions yielding

$$\Gamma = \int_0^\infty [c_m(x) - \phi_b^2]\,dx \simeq Dc_M \simeq \frac{|y_s|^{3/2}}{l_B a f^{1/2}} \sim \frac{|\psi_s|^{3/2}}{f^{1/2}} \quad (63)$$

The adsorbed amount $\Gamma(f)$ in the low-salt regime is plotted in the inset of Fig. 13(a). As a consequence of Eq. (63), Γ decreases with increasing charge fraction f. Similar behavior was also reported in experiments [106]. This effect is at first glance quite puzzling because as the polymer charge increases, the chains are subject to a stronger attraction to the surface. On the other hand, the monomer–monomer repulsion is stronger and, indeed, in this regime, the monomer–monomer Coulomb repulsion scales as $(fc_M)^2$ and dominates over the adsorption energy that scales as fc_M.

2.7.5.3.2 **High-salt Regime $D \gg \kappa^{-1}$ and ψ_s = constant** Let us now consider the opposite case of a high ionic strength solution. Here, D is much larger than κ^{-1}, and the electrostatic interactions are short ranged with a cutoff κ^{-1}. The free energy of the adsorbing PE layer (per unit surface area) then reads

$$F \simeq \frac{a^2}{6D} c_M - f|y_s|c_M\kappa^{-1} + 4\pi l_B f^2 \kappa^{-2} c_M^2 D + \frac{1}{2} v_2 c_M^2 D \quad (64)$$

The electrostatic cutoff enters in two places. In the second term, only the first layer of width κ^{-1} interacts electrostatically with the surface. In the third term, each charged layer situated at point x interacts only with layers at x' for which $|x - x'| < \kappa^{-1}$. This term can be also viewed as an additional electrostatic excluded volume with $v_{el} \sim l_B(f/\kappa)^2$.

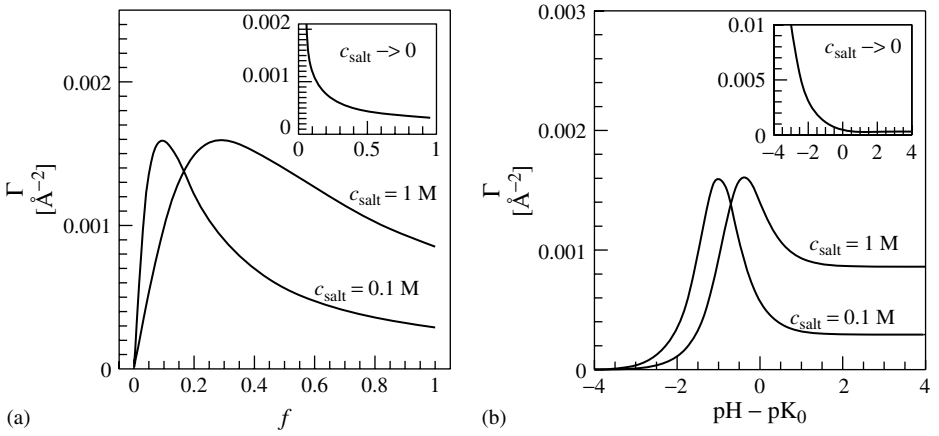

Fig. 13 Typical adsorbed amount Γ as a function of (a) the charge fraction f and (b) the pH − pK$_0$ of the solution for different salt concentrations (Eq. 67). The insets correspond to the low-salt regime (Eq. 63). The parameters used for ε, T, and ν_2 are the same as in Fig. 11, while $\gamma_s = e\psi_s/k_BT = -0.5$ and $a = 5$Å. The bulk concentration $c_m^b = \phi_b^2$ is assumed to be much smaller than c_M. (Adapted from Ref. [124].)

Minimization of the free energy gives

$$D \simeq \frac{\kappa a^2}{f|\gamma_s|} \sim \frac{c_{salt}^{1/2}}{f|\psi_s|} \tag{65}$$

and

$$c_M \sim \frac{f^2|\gamma_s|^2/(\kappa a)^2}{f^2/c_{salt} + \alpha\nu_2} \tag{66}$$

yielding

$$\Gamma \sim \frac{f|\gamma_s|c_{salt}^{-1/2}}{f^2/c_{salt} + \alpha\nu_2} \sim \frac{f|\psi_s|}{\nu_{el} + \alpha\nu_2} c_{salt}^{-1/2} \tag{67}$$

where α is a numerical constant of order unity that depends on the profile details.

The adsorption behavior is depicted in Figs. 13 and 14. Our scaling results are in agreement with numerical solutions of discrete lattice models (the multi-Stern layer theory) [61, 62, 111, 117–120]. In Fig. 13, Γ is plotted as function of f (Fig. 13a) and the pH (Fig. 13b) for different salt concentrations. The behavior as seen in Fig. 13(b) represents annealed PEs where the nominal charge fraction is given by the pH of the solution through the expression

$$f = \frac{10^{pH-pK_0}}{1 + 10^{pH-pK_0}} \tag{68}$$

where $pK_0 = -\log_{10} K_0$ and K_0 is the apparent dissociation constant. We note that this relation is only strictly valid for infinitely dilute monomers and that distinct deviations from it are observed for PEs because of the electrostatic repulsion between neighboring dissociating sites [126]. Still, the results in Fig. 13(b) capture the main qualitative trends of pH-dependent PE adsorption.

Another interesting observation that can be deduced from Eq. (67) is that Γ is only a function of $f c_{salt}^{-1/2}$. Indeed, as can be seen in Fig. 13, c_{salt} only affects the position of the peak and not its height.

The effect of salt concentration is shown in Fig. 14, where Γ is plotted as function of the salt concentration c_{salt} for two charge fractions $f = 0.01$ and 0.25. The curves on the right-hand side of the graph are

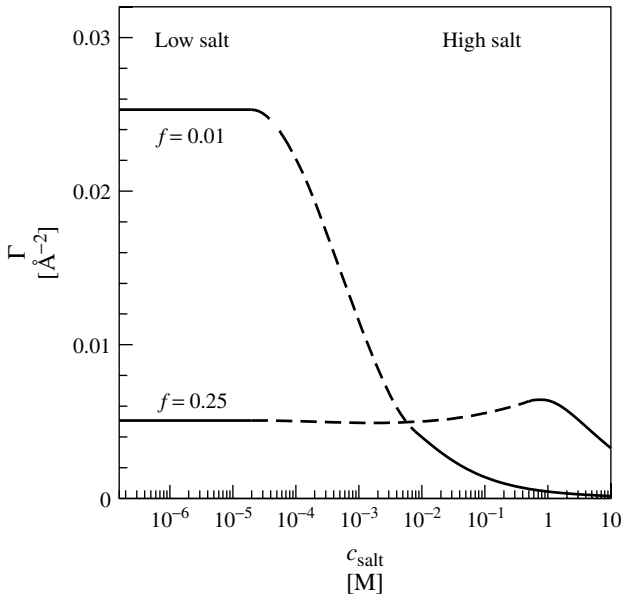

Fig. 14 The adsorbed amount Γ as a function of the salt concentration c_{salt} (Eq. 67) for $f = 0.01$ and 0.25. The solid curves on the right-hand side correspond to the scaling relations in the high-salt regime (Eq. 67). The horizontal lines on the left-hand side mark the low salt values (Eq. 67). The dashed lines serve as guides to the eye. The parameters used are $\varepsilon = 80$, $T = 300$ K, $\nu_2 = 50$Å^3, $a = 5$Å, $\gamma_s = -2.0$. (Adapted from Ref. [124].)

calculated from the high-salt expression for Γ (Eq. 67). The horizontal lines on the left-hand side of the graph indicate the low-salt values of Γ (Eq. 63). The dashed lines in the intermediate salt regime serve only as guides to the eye since our scaling approach is not valid when D and κ^{-1} are of the same order.

Emphasis should be drawn to the distinction between weakly and strongly charged PEs. For weak PEs, the adsorbed amount Γ is a monotonously decreasing function of the salt concentration c_{salt} in the whole range of salt concentrations. The reason being that the monomer–monomer Coulomb repulsion, proportional to f^2, is weaker than the monomer–surface interaction, which is linear in f.

For strongly charged PEs, on the other hand, the balance between these two electrostatic terms depends on the amount of salt. At low salt concentrations, the dominant interaction is the monomer–surface Coulomb repulsion. Consequently, addition of salt screens this interaction and increases the adsorbed amount. When the salt concentration is high enough, this Coulomb repulsion is screened out and the effect of salt is to weaken the surface attraction. At this point the adsorbed amount starts to decrease. As a result, the behavior over the whole concentration range is nonmonotonic with a maximum at some optimal value c^*_{salt}, as seen in Fig. 14.

From this analysis and from Figs. 13, 14 and Eq. (67), it is now natural to divide the high-salt regime into two subregimes

according to the PE charge. At low charge fractions (subregime HS I), $f \ll f^* = (c_{salt}\upsilon_2)^{1/2}$, the excluded volume term dominates the denominator of Eq. (67) and

$$\Gamma \sim f|\psi_s|c_{salt}^{-1/2} \tag{69}$$

whereas at high f (subregime HS II), $f \gg f^*$, the monomer–monomer electrostatic repulsion dominates and Γ decreases with f and increases with c_{salt}:

$$\Gamma \sim c_{salt}^{1/2}|\psi_s|f^{-1} \tag{70}$$

The various regimes with their crossover lines are shown schematically in Fig. 15. Keeping the charge fraction f constant while changing the amount of salt corresponds to a vertical scan through the diagram. For weak PEs, this cut goes through the left-hand side of the diagram starting from the low-salt regime and, upon addition of salt, into the HS I regime. Such a path describes the monotonous behavior inferred from Fig. 14 for the weak PE ($f = 0.01$). For strong PEs, the cut goes through the right-hand side of the diagram, starting from the low-salt regime, passing through the HS II regime, and ending in the HS I. The passage through the HS II regime is responsible for the nonmonotonous behavior inferred from Fig. 14 for the strong PE ($f = 0.25$).

Similarly, Fig. 13(a,b) correspond to horizontal scans through the top half of the diagram. As long as the system is in the HS I regime, the adsorbed amount increases when the polymer charge fraction

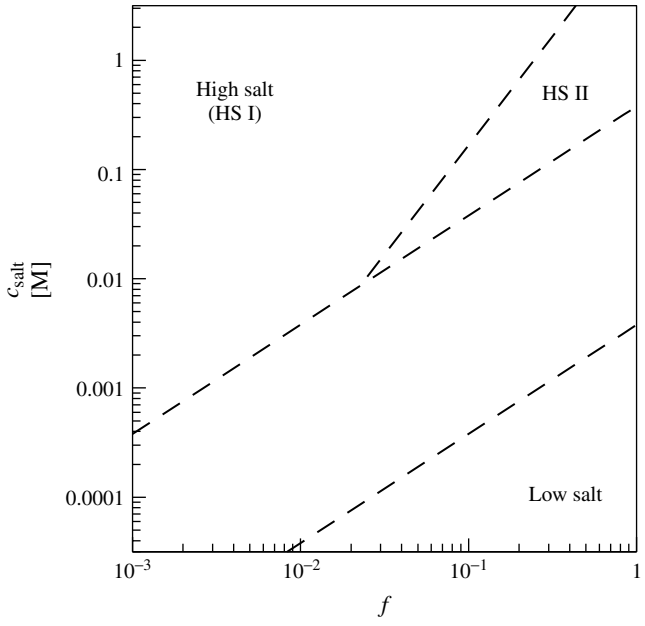

Fig. 15 Schematic diagram of the different adsorption regimes as function of the charge fraction f and the salt concentration c_{salt}. Three regimes can be distinguished: (a) the low-salt regime $D \ll \kappa^{-1}$; (b) the high-salt regime (HS I) $D \gg \kappa^{-1}$ for weak PEs $f \ll f^* = (c_{salt}\upsilon_2)^{1/2}$; and (c) the high-salt regime (HS II) $D \gg \kappa^{-1}$ for strong PEs $f \gg f^*$.

increases. As the polymer charge further increases, the system enters the HS II regime and the adsorbed amount decreases. Thus, the nonmonotonous behavior of Fig. 13. We finally note that the single-chain desorption transition for a flexible chain, which was discussed in Sect. 2.7.4, is also valid for adsorption from solutions and will lead to a desorption transition at very high salt concentrations in Fig. 15 (which is not shown for clarity).

2.7.5.4 Overcompensation of Surface Charges: Constant σ

We turn now to a different electrostatic boundary condition of constant surface charge density and look at the interesting phenomenon of charge compensation by the PE chains in relation to experiments for PE adsorption on flat surfaces, as well as on charged colloidal particles [72, 73, 75–77]. What was observed in experiments is that PEs adsorbing on an oppositely charged surface can overcompensate the original surface charge. Because PEs create a thin layer close to the surface, they can act as an effective absorbing surface to a second layer of PEs having an opposite charge compared to the first layer. Repeating the adsorption of alternating positively and negatively charged PEs, it is possible to create a multilayer structure of PEs at the surface. Although many experiments and potential applications for PE multilayers exist, the theory of PE overcompensation is only starting to be developed [83, 84, 123–125, 127, 128].

The scaling laws presented for constant ψ_s can be used also for the case of constant surface charge. A surface held at a constant potential ψ_s will induce a surface charge density σ. The two quantities are related by $\mathrm{d}\psi/\mathrm{d}x = 4\pi\sigma e/\varepsilon$ at $x = 0$. We will now consider separately the two limits: low salt $D \ll \kappa^{-1}$ and high salt $D \gg \kappa^{-1}$.

2.7.5.4.1 **Low Salt Limit: $D \ll \kappa^{-1}$** Assuming that there is only one length scale characterizing the potential behavior in the vicinity of the surface, as demonstrated in Fig. 12(a), we find that the surface potential ψ_s and the surface charge σ are related by $\psi_s \sim \sigma e D$. In the low salt limit we find from Eq. (61)

$$D \sim (f\sigma l_\mathrm{B})^{-1/3} \tag{71}$$

in agreement with Eq. (47).

Let us define two related concepts via the effective surface charge density defined as $\Delta\sigma = f\Gamma - \sigma$, which is the sum of the adsorbed polymer charge density and the charge density of the bare substrate. For $\Delta\sigma = 0$, the adsorbed polymer charge exactly *compensates* the substrate charge. If $\Delta\sigma$ is positive, the PE *overcompensates* the substrate charge and more polymer adsorbs than is needed to exactly cancel the substrate charge. If $\Delta\sigma$ is positive and reaches the value $\Delta\sigma = \sigma$, it means that the PE charge is $f\Gamma = 2\sigma$ and leads to a *charge inversion* of the substrate charge. The effective surface charge consisting of the substrate charge and the PE layer has a charge density that is exactly opposite to the original substrate charge density σ.

Do we obtain overcompensation or charge inversion in the low salt limit within mean-field theory? Using scaling arguments, this is not clear since we find that $\Delta\sigma \sim f\Gamma \sim \sigma$. That is, each of the two terms in $\Delta\sigma$ scales linearly with σ, and the occurrence of overcompensation or charge inversion will depend on numerical prefactors determining the relative sign of the two opposing terms. However, if we look at the numerical solution for the mean-field electrostatic potential (Fig. 12), we see indeed that all plotted profiles have a maximum of $\psi(x)$ as function of x. An extremum in ψ means a zero local electric

field. Or equivalently, using Gauss law, this means that the integrated charge density from the wall to this special extremum point (including surface charges) is exactly zero. At this point the charges in solution exactly compensate the surface charges.

2.7.5.4.2 High Salt Limit: $D \gg \kappa^{-1}$

When we include salt in the solution and look at the high salt limit, the situation is more complex. The only length characterizing the exponential decay of ψ close to the surface is the DH screening length. Hence, using $\mathrm{d}\psi/\mathrm{d}x|_s \sim \sigma e$ yields $\psi_s \sim \sigma e \kappa^{-1}$, and therefore from Eq. (65),

$$D \sim \frac{\kappa^2 a^2}{f \sigma l_B} \sim \kappa^2 f^{-1} \sigma^{-1} \qquad (72)$$

The estimation of the PE layer charge can be obtained by using the expression for D and c_M in this high salt limit (Eqs. 63–65), yielding

$$f\Gamma \simeq \frac{\beta\sigma\ (8\pi l_B c_{salt} \kappa^{-2})}{1 + \alpha v_2 c_{salt} f^{-2}} = \frac{\beta\sigma}{1 + v_2/v_{el}} \qquad (73)$$

where $v_{el} = f^2/\alpha c_{salt}$ is the electrostatic contribution to the second-virial coefficient v_2 and $\alpha > 0$ and $\beta > 1$ are positive numerical factors.

We see that $\Delta\sigma = f\Gamma - \sigma$ is a decreasing function of v_2. Charge overcompensation can occur when v_2 is smaller than v_{el} (up to a prefactor of order unity). When v_2 can be neglected in the vicinity of the surface, or when $v_2 = 0$ (theta solvents), there is always charge overcompensation, $\Delta\sigma = (\beta - 1)\sigma > 0$. This is the case of strongly charged PEs. Similar conclusions have been mentioned in Refs. [83, 127] where v_2 was taken as zero but the surface has a nonelectrostatic short range interaction with the PE. By tuning the relative strength of the surface charge density σ and the nonelectrostatic interaction, it is also possible to cause a charge overcompensation and even an exact charge inversion in a special case.

Finally, we note that the dependence of the charge parameter $\Delta\sigma$ on the amount of salt, c_{salt}, is different for constant surface charge and constant surface potential cases. While for the former, $\Delta\sigma$ is nonmonotonous and has a maximum (as mentioned above) as function of the salt concentration, in the latter case, $\Delta\sigma/\sigma$ is a monotonic decreasing function of c_{salt} (Eq. 73). This can be explained by the extra powers of c_{salt} in the latter case coming from the relation $\psi_s \sim \sigma c_{salt}^{-1/2} \sim \sigma\kappa^{-1}$.

Let us remark that in other theories the overcharging is due to lateral correlations between adsorbed PEs, which in conjunction with screening by salt ions leads to strongly overcharged surfaces [84, 128].

2.7.5.5 Final Remarks on Adsorption from Semidilute Solutions

The results presented earlier (Sect. 2.7.5) for adsorption from solutions have been derived using mean-field theory. Hence, lateral fluctuations in the polymer and ionic concentrations are neglected. In addition, we neglect the delicate influence of the charges on the PE persistence length and any deviations from ground state dominance [9]. The region of validity of the theory is for long and weakly charged polymer chains in contact with a moderately charged surface. The PE solution is placed in contact with a single and ideal surface (infinite, flat, and homogeneous). The problem reduces then to an effective one-dimensional problem depending only on the distance from the charged surface. We take very simple boundary conditions for the surface assuming that the polymer concentration is zero on the

surface and keeping the surface in constant potential or constant surface charge conditions.

We find numerical solutions for the PE profile equations in various cases. These numerical solutions agree well with simple scaling assumptions describing the adsorption of PEs. Scaling expressions for the amount of adsorbed polymer Γ and the width D of the adsorbed layer, as a function of the fractional charge f and the salt concentration c_{salt}, are obtained for two cases: constant ψ_s and constant σ.

For constant ψ_s and in the low-salt regime, a $f^{-1/2}$ dependence of Γ is found. It is supported by our numerical solutions of the profile Eqs. (55) and (56) and is in agreement with experiment [106]. This behavior is due to strong Coulomb repulsion between adsorbed monomers in the absence of salt. As f decreases, the adsorbed amount increases until the electrostatic attraction becomes weaker than the excluded volume repulsion, at which point, Γ starts to decrease rapidly.

At high salt concentrations it is not possible to neglect the excluded volume interaction of the monomers since the electrostatic interactions are screened by the salt. We obtain two limiting behaviors: (1) For weakly charged PEs, $f \ll f^* = (c_{\text{salt}} v_2)^{1/2}$, the adsorbed amount increases with the fractional charge and decreases with the salt concentration, $\Gamma \sim f/\sqrt{(c_{\text{salt}})}$, owing to the monomer–surface electrostatic attraction. (2) For strong PEs, $f \gg f^*$, the adsorbed amount decreases with the fractional charge and increases with the salt concentration, $\Gamma \sim \sqrt{(c_{\text{salt}})}/f$, owing to the dominance of monomer–monomer electrostatic repulsion. Between these two regimes, we find that the adsorbed amount reaches a maximum in agreement with experiments [107, 110].

The scaling arguments are then repeated for constant σ boundary conditions. It is found that the PE can possibly cause charge overcompensation and even inversion of the nominal substrate charge, leading the way to multilayer formation of positively and negatively charged PEs. The scaling approach can serve as a starting point for further investigations. The analytical and approximated expressions are valid only in specific limits. Special attention should be directed to the crossover regime where D and κ^{-1} are of comparable size.

The problem of charge inversion is not well understood at present. Alternative approaches rely on lateral correlations between semiflexible adsorbed PE chains, which also can lead to strong overcompensation of surface charges [84, 128].

2.7.6 Polyelectrolyte Brushes

Charged polymers that are densely endgrafted to a surface are called *polyelectrolyte brushes* or *charged brushes*. They have been the focus of numerous theoretical [129–138] and experimental [139–142] studies. In addition to the basic interest, charged brushes are considered for their applications as efficient means for preventing colloids in polar media (such as aqueous solutions) from flocculating and precipitating out of solution [93]. This stabilization arises from steric (entropic) and electrostatic (energetic) repulsion. A strongly charged brush is able to trap its own counterions and generates a layer of locally enhanced salt concentration [131]. It is thus less sensitive to the salinity of the surrounding aqueous medium than a stabilization mechanism based on pure electrostatics (i.e. without polymers).

Neutral brushes have been extensively studied theoretically in the past using scaling theories [143, 144], strong-stretching theories [145–149], self-consistent field theories [150, 151], and computer simulations [152–155]. Little is known from experiments on the scaling behavior of PE brushes as compared to uncharged polymer brushes. The thickness of the brush layer has been calculated from neutron-scattering experiments on end-grafted polymers [139] and charged diblock copolymers at the air–water interface [141, 142].

Theoretical work on PE brushes was initiated by the works of Miklavic and Marcelja [129] and Misra and coworkers. [130]. In 1991, Pincus [131] and Borisov, Birshtein and Zhulina [132] presented scaling theories for charged brushes in the so-called osmotic regime, where the brush height results from the balance between the chain elasticity (which tends to decrease the brush height) and the repulsive osmotic counterion pressure (which tends to increase the brush height). In later studies, these works have been generalized to the poor solvents [133, 134] and to the regime where excluded volume effects become important, that is, the so-called quasi-neutral or Alexander regime [137].

In what follows we assume that the charged brush is characterized by two length scales: the average vertical extension of polymer chains from the wall L and the typical extent of the counterion cloud, denoted by H. We neglect the presence of additional salt, which has been discussed extensively in the original literature, and only consider screening effects due to the counterions of the charged brush. Two different scenarios emerge, as is schematically presented in Fig. 16. The counterions can either extend outside the brush, $H \gg L$, as shown in Fig. 16(a), or be confined inside the brush, $H \approx L$, as shown in Fig. 16(b). As we show now, case (b) is indicative of strongly charged brushes, while case (a) is typical for weakly charged brushes.

The free energy per unit area (and in units of $k_B T$) contains several contributions. We denote the grafting density of PEs by ρ, the counterion valency by z, recalling that N is the polymerization index of grafted chains and f their charge fraction. The osmotic free energy, F_{os}, associated with the ideal entropy cost of confining the counterions to a layer of thickness H is given by

$$F_{os} \simeq \frac{Nf\rho}{z} \ln\left(\frac{Nf\rho}{zH}\right) \qquad (74)$$

F_{v_2} is the second-virial contribution to the free energy, arising from steric repulsion between the monomers (contributions due to counterions are neglected). Throughout this review, the polymers are assumed to be in a good solvent (positive second-virial coefficient $v_2 > 0$). The contribution thus reads

$$F_{v_2} \simeq \frac{1}{2} L v_2 \left(\frac{N\rho}{L}\right)^2 \qquad (75)$$

Finally, a direct electrostatic contribution F_{el} occurs if the PE brush is not locally electro-neutral throughout the system, as for example is depicted in Fig. 16(a). This energy is given by

$$F_{el} = \frac{2\pi \ell_B (Nf\rho)^2}{3} \frac{(L-H)^2}{H} \qquad (76)$$

This situation arises in the limit of low charge, when the counterion density profile extends beyond the brush layer, that is, $H > L$.

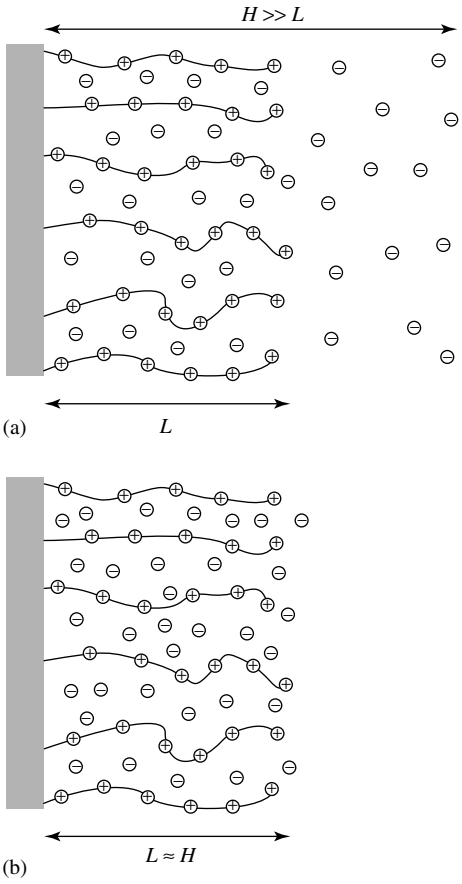

Fig. 16 Schematic PE brush structure. In (a), we show the weak-charge limit where the counterion cloud has a thickness H larger than the thickness of the brush layer, L. In (b), we show the opposite case of the strong-charge limit, where all counterions are contained inside the brush and a single length scale $L \approx H$ exists.

The last contribution is the stretching energy of the chains, which is

$$F_{\mathrm{st}} = \frac{3L^2}{2Na^2}\rho \tag{77}$$

Here, a is the monomer size or Kuhn length of the polymer, implying that we neglect any chain stiffness for the brush problem. The different free energy contributions lead, upon minimization with respect to the two length scales H and L, to different behaviors. Let us first consider the weak charging limit, that is, the situation in which the counterions leave the brush, $H > L$. In this case, minimization of $F_{\mathrm{os}} + F_{\mathrm{el}}$ with respect to the counterion height H leads to

$$H \sim \frac{1}{z\ell_{\mathrm{B}}Nf\rho} \tag{78}$$

which is the Gouy-Chapman length for z-valent counterions at a surface of surface charge density $\sigma = Nf\rho$. Balancing now the polymer stretching energy F_{st} and the electrostatic energy F_{el}, one obtains the so-called Pincus brush

$$L \simeq N^3\rho a^2\ell_{\mathrm{B}}f^2 \tag{79}$$

In the limit of $H \approx L$, the PE brush can be considered as neutral and the

electrostatic energy vanishes. There are two ways of balancing the remaining free energy contributions. The first is obtained by comparing the osmotic energy of counterion confinement, F_{os}, with the polymer stretching term, F_{st}, leading to the height

$$L \sim \frac{Naf^{1/2}}{z^{1/2}} \tag{80}$$

constituting the so-called osmotic-brush regime. Finally, comparing the second-virial free energy, F_{v_2}, with the polymer stretching energy, F_{st}, one obtains

$$L \sim Na(v_2\rho/a)^{1/3} \tag{81}$$

and the PE brush is found to have the same scaling behavior as the neutral brush [143, 144]. Comparing the heights of all three regimes, we arrive at the phase diagram shown in Fig. 17. The three scaling regimes meet at the characteristic charge fraction

$$f^* \sim \left(\frac{zv_2}{N^2a^2\ell_B}\right)^{1/3} \tag{82}$$

and the characteristic grafting density

$$\rho^* \sim \frac{1}{N\ell_B^{1/2}v_2^{1/2}} \tag{83}$$

For large values of the charge fraction f and the grafting density ρ, it has been found numerically that the brush height does not follow any of the scaling laws discussed here [156]. This has been recently rationalized in terms of another scaling regime, the collapsed regime. In this regime, one finds that correlation and fluctuation effects, which are neglected in the discussion in this section, lead to a net attraction between charged monomers and counterions [157].

2.7.7 Conclusion

In this chapter we have reviewed the behavior of charged polymers (PEs) in solution and at interfaces, concentrating on aspects that are different from the corresponding behavior of neutral polymers.

Because charged biopolymers and isolated PE chains tend to be quite stiff due to electrostatic monomer–monomer

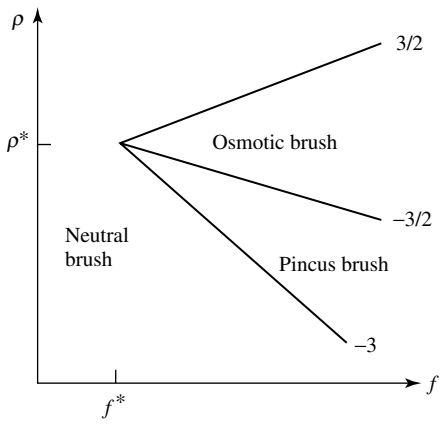

Fig. 17 Scaling diagram for PE brushes on a log–log plot as a function of the grafting density ρ and the fraction of charged monomers f. Featured are the Pincus-brush regime, where the counterion layer thickness is much larger than the brush thickness, the osmotic-brush regime, where all counterions are inside the brush and the brush height is determined by an equilibrium between the counterion osmotic pressure and the PE stretching energy, and the neutral-brush regime, where charge effects are not important and the brush height results from a balance of PE stretching energy and second-virial repulsion. The power-law exponents of the various lines are denoted by numbers.

repulsions, their chain statistics is related to that of semiflexible polymers. Neutral and charged semiflexible polymers are controlled by their bending rigidity, which is usually expressed in terms of a persistence length (see Sect. 2.7.2.2). For PEs, the electrostatic interaction considerably influences this persistence length.

In solution, we have considered the scaling behavior of a single PE (Sect. 2.7.3.1). The importance of the electrostatic persistence length was stressed. The Manning condensation of counterions leads to a reduction of the effective linear charge density (Sect. 2.7.3.1.1). Excluded volume effects are typically less important than for neutral polymers (Sect. 2.7.3.1.2). Dilute PE solutions are typically dominated by the behavior of the counterions. So is the large osmotic pressure of dilute PE solutions due to the entropic contribution of the counterions (Sect. 2.7.3.2). Semidilute PE solutions can be described by the RPA, which in particular yields the characteristic peak of the structure factor.

At surfaces, we discussed in detail the adsorption of single PEs (Sect. 2.7.4), the adsorption from semidilute solutions (Sect. 2.7.5), and the behavior of end-grafted PE chains (Sect. 2.7.6). We tried to express the PE behavior in terms of a few physical parameters such as the chain characteristics (persistence length), ionic strength of the solutions, and surface characteristics. The shape and size of the adsorbing layer is, in many instances, governed by a delicate balance of competing mechanisms of electrostatic and nonelectrostatic origin. In some cases, it is found that the adsorbing PE layer is flat and compressed, while in other cases, it is coiled and extended. Yet, in other situations, the PEs will not adsorb at all and will be depleted from the surface. We also briefly review the phenomenon of charge overcompensation and inversion, when the adsorbed PE layer effectively inverses the sign of the surface charge leading the way to formation of PE multilayers.

Important topics that we have left out are the dynamics of PE solutions, which is reviewed in Ref. [4], and the behavior of PEs under bad-solvent conditions [39–41]. In the future we expect that studies of PEs in solutions and at surfaces will be directed more toward biological systems. We mentioned in this review the complexation of DNA and histones (Sect. 2.7.4.1). This is only one of many examples of interest in which charged biopolymers, receptors, proteins, and DNA molecules interact with each other or with other cellular components. The challenge for future fundamental research will be to try to understand the role of electrostatic interactions combined with specific biological (lock–key) mechanisms and to infer on biological functionality of such interactions.

Acknowledgment

It is a pleasure to thank our collaborators I. Borukhov, J.F. Joanny, K. Kunze, L. Leibler, R. Lipowsky, H. Orland, M. Schick, and C. Seidel with whom we have been working on PE problems. We benefitted from discussions with G. Ariel, Y. Burak, and M. Ullner. One of us (DA) would like to acknowledge partial support from the Israel Science Foundation funded by the Israel Academy of Sciences and Humanities – Centers of Excellence Program and the Israel–US Binational Science Foundation (BSF) under grant no. 98-00429.

References

1. F. Oosawa, *Polyelectrolytes*, Marcel Dekker, New York, 1971.
2. H. Dautzenberg, W. Jaeger, B. P. J. Kötz et al., *Polyelectrolytes: Formation, characterization and application*, Hanser Publishers, Munich, 1994.
3. S. Förster, M. Schmidt, *Adv. Polym. Sci.* **1995**, *120*, 50.
4. J.-L. Barrat, J.-F. Joanny, *Adv. Chem. Phys.* **1996**, *94*, 1.
5. E. Eisenriegler, *Polymers Near Surfaces*, World Scientific, Singapore, 1993.
6. A. Yu. Grosberg, A. R. Khokhlov, *Statistical Physics of Macromolecules*, AIP Press, New York, 1994.
7. P. J. Flory, *Principles of Polymer Chemistry*, Cornell University, Ithaca, 1953.
8. H. Yamakawa, *Modern Theory of Polymer Solutions*, Harper and Row, New York, 1971.
9. P. G. de Gennes, *Scaling Concepts in Polymer Physics*, Cornell University, Ithaca, 1979.
10. A. R. Khokhlov, K. A. Khachaturian, *Polymer* **1982**, *23*, 1742.
11. J.-L. Barrat, J.-F. Joanny, *Europhys. Lett.* **1993**, *24*, 333.
12. R. R. Netz, H. Orland, *Eur. Phys. J. B* **1999**, *8*, 81.
13. T. Odijk, *J. Polym. Sci., Polym. Phys. Ed.* **1977**, *15*, 477.
14. T. Odijk, *Polymer* **1978**, *19*, 989.
15. J. Skolnick, M. Fixman, *Macromolecules* **1977**, *10*, 944.
16. G. A. Christos, S. L. Carnie, *J. Chem. Phys.* **1990**, *92*, 7661.
17. C. Seidel, H. Schlacken, I. Müller, *Macromol. Theory Simul.* **1994**, *3*, 333.
18. M. Ullner, B. Jönsson, C. Peterson et al., *J. Chem. Phys.* **1997**, *107*, 1279.
19. U. Micka, K. Kremer, *Phys. Rev. E* **1996**, *54*, 2653.
20. U. Micka, K. Kremer, *Europhys. Lett.* **1997**, *38*, 279.
21. H. Li, T. Witten, *Macromolecules* **1995**, *28*, 5921.
22. B.-Y. Ha, D. Thirumalai, *J. Chem. Phys.* **1999**, *110*, 7533.
23. B.-Y. Ha, D. Thirumalai, *Macromolecules* **1995**, *28*, 577.
24. T. B. Liverpool, M. Stapper, *Europhys. Lett.* **1997**, *40*, 485.
25. R. G. Winkler, M. Gold, P. Reineker, *Phys. Rev. Lett.* **1998**, *80*, 3731.
26. N. V. Brilliantov, D. V. Kuznetsov, R. Klein, *Phys. Rev. Lett.* **1998**, *81*, 1433.
27. M. O. Khan, B. Jönsson, *Biopolymers* **1999**, *49*, 121.
28. T. T. Nguyen, I. Rouzina, B. I. Shklovskii, *Phys. Rev. E* **1999**, *60*, 7032.
29. G. S. Manning, *J. Chem. Phys.* **1969**, *51*, 924.
30. G. S. Manning, *J. Chem. Phys.* **1969**, *51*, 934.
31. G. S. Manning, U. Mohanty, *Physica A* **1997**, *247*, 196.
32. M. Deserno, C. Holm, S. May, *Macromolecules* **2000**, *33*, 199.
33. C. Wandrey, D. Hunkeler, U. Wendler et al., *Macromolecules* **2000**, *33*, 7136.
34. J. Blaul, M. Wittemann, M. Ballauff et al., *J. Phys. Chem. B* **2000**, *104*, 7077.
35. H. Schiessel, P. Pincus, *Macromolecules* **1998**, *31*, 7953.
36. H. Schiessel, *Macromolecules* **1999**, *32*, 5673.
37. A. R. Khokhlov, *J. Phys. A* **1980**, *13*, 979.
38. Y. Kantor, M. Kardar, *Phys. Rev. E* **1995**, *51*, 1299.
39. A. V. Dobrynin, M. Rubinstein, S. P. Obukhov, *Macromolecules* **1996**, *29*, 2974.
40. A. L. Lyulin, B. Dünweg, O. V. Borisov et al., *Macromolecules* **1999**, *32*, 3264.
41. U. Micka, C. Holm, K. Kremer, *Langmuir* **1999**, *15*, 4033.
42. T. A. Waigh, R. Ober, C. E. Williams et al., *Macromolecules* **2001**, *34*, **1973**.
43. M. Nierlich, F. Boue, A. Lapp et al., *Coll. Polym. Sci.* **1985**, *263*, 955.
44. M. Nierlich, F. Boue, A. Lapp et al., *J. Phys. (France)* **1985**, *46*, 649.
45. A. Moussaid, F. Schosseler, J. P. Munch et al., *J. Phys. II (France)* **1993**, *3*, 573.
46. W. Essafi, F. Lafuma, C. E. Williams, *J. Phys. II (France)* **1995**, *5*, 1269.
47. K. Nishida, K. Kaji, T. Kanaya, *Macromolecules* **1995**, *28*, 2472.
48. W. Essafi, F. Lafuma, C. E. Williams, *Eur. Phys. J. B* **1999**, *9*, 261.
49. V. Y. Borue, I. Y. Erukhimovich, *Macromolecules* **1988**, *21*, 3240.
50. J. F. Joanny, L. Leibler, *J. Phys. (France)* **1990**, *51*, 545.
51. J. des Cloizeaux, *Macromolecules* **1973**, *6*, 403.
52. T. Yoshizaki, H. Yamakawa, *Macromolecules* **1980**, *13*, 1518.
53. R. R. Netz, to be published.
54. M. N. Spiteri, F. Boue, A. Lapp et al., *Phys. Rev. Lett.* **1996**, *77*, 5218.

55. T. A. Witten, P. Pincus, *Europhys. Lett.* **1987**, *3*, 315.
56. J.-L. Barrat, J.-F. Joanny, *J. Phys. II (France)* **1994**, *4*, 1089.
57. M. J. Stevens, K. Kremer, *J. Chem. Phys.* **1995**, *103*, 1669.
58. M. J. Stevens, K. Kremer, *J. Phys. II (France)* **1996**, *6*, 1607.
59. H. Schäfer, C. Seidel, *Macromolecules* **1997**, *30*, 6658.
60. M. J. Stevens, S. J. Plimpton, *Eur. Phys. J. B* **1998**, *2*, 341.
61. M. A. Cohen Stuart, *J. Phys. (France)* **1988**, *49*, 1001.
62. M. A. Cohen Stuart, G. J. Fleer, J. Lyklema, et al., *Adv. Colloid Interface Sci.* **1991**, *34*, 477.
63. Y. Fang, J. Yang, *J. Phys. Chem. B* **1997**, *101*, 441.
64. J. O. Rädler, I. Koltover, T. Salditt et al., *Science* **1997**, *275*, 810.
65. T. Salditt, I. Koltover, J. O. Rädler et al., *Phys. Rev. Lett.* **1997**, *79*, 2582.
66. B. Maier, J. O. Rädler, *Phys. Rev. Lett.* **1999**, *82*, 1911.
67. H. von Berlepsch, C. Burger, H. Dautzenberg, *Phys. Rev. E* **1998**, *58*, 7549.
68. K. de Meijere, G. Brezesinski, H. Möhwald, *Macromolecules* **1997**, *30*, 2337.
69. G. Decher, J. D. Hong, J. Schmitt, *Thin Solid Films* **1992**, *210/211*, 831.
70. R. von Klitzing, H. Möhwald, *Langmuir* **1995**, *11*, 3554.
71. R. von Klitzing, H. Möhwald, *Macromolecules* **1996**, *29*, 6901.
72. G. Decher, *Science* **1997**, *277*, 1232.
73. M. Lösche, J. Schmitt, G. Decher et al., *Macromolecules* **1998**, *31*, 8893.
74. F. Caruso, K. Niikura, D. N. Furlong et al., *Langmuir* **1997**, *13*, 3422.
75. E. Donath, G. B. Sukhorukov, F. Caruso et al., *Angew. Chem., Int. Ed.* **1998**, *110*, 2323.
76. G. B. Sukhorukov, E. Donath, S. A. Davis et al., *Polym. Adv. Technol.* **1998**, *9*, 759.
77. F. Caruso, R. A. Caruso, H. Möhwald, *Science* **1998**, *282*, 1111.
78. M. Muthukumar, *J. Chem. Phys.* **1987**, *86*, 7230.
79. X. Chatellier, J.-F. Joanny, *J. Phys. II (France)* **1996**, *6*, 1669.
80. R. Varoqui, *J. Phys. (France) II* **1993**, *3*, 1097.
81. I. Borukhov, D. Andelman, H. Orland, *Europhys. Lett.* **1995**, *32*, 499.
82. I. Borukhov, D. Andelman, H. Orland in *Short and Long Chains at Interfaces* (Eds.: J. Daillant, P. Guenoun, C. Marques et al.), Edition Frontieres, Gif-sur-Yvette, 1995, pp. 13–20.
83. J. F. Joanny, *Eur. Phys. J. B* **1999**, *9*, 117.
84. R. R. Netz, J. F. Joanny, *Macromolecules* **1999**, *32*, 9013.
85. O. V. Borisov, E. B. Zhulina, T. M. Birshtein, *J. Phys. II (France)* **1994**, *4*, 913.
86. T. Odijk, *Macromolecules* **1983**, *16*, 1340.
87. T. Odijk, *Macromolecules* **1984**, *17*, 502.
88. A. C. Maggs, D. A. Huse, S. Leibler, *Europhys. Lett.* **1989**, *8*, 615.
89. G. Gompper, T. W. Burkhardt, *Phys. Rev. A* **1989**, *40*, 6124.
90. G. Gompper, U. Seifert, *J. Phys. A* **1990**, *23*, L1161.
91. R. Bundschuh, M. Lässig, R. Lipowsky, *Eur. Phys. J. E* **2000**, *3*, 295.
92. V. Yamakov, A. Milchev, O. Borisov et al., *J. Phys.: Condens. Matter* **1999**, *11*, 9907.
93. D. H. Napper, *Polymeric Stabilization of Colloidal Dispersions*, Academic Press, New York, 1983.
94. T. Wallin, P. Linse, *Langmuir* **1996**, *12*, 305.
95. T. Wallin, P. Linse, *J. Phys. Chem.* **1996**, *100*, 17 873.
96. T. Wallin, P. Linse, *J. Phys. Chem. B* **1997**, *101*, 5506.
97. E. M. Mateescu, C. Jeppesen, P. Pincus, *Europhys. Lett.* **1999**, *46*, 493.
98. R. R. Netz, J. F. Joanny, *Macromolecules* **1999**, *32*, 9026.
99. K. K. Kunze, R. R. Netz, *Phys. Rev. Lett.* **2000**, *85*, 4389.
100. T. D. Yager, C. T. McMurray, K. E. van Holde, *Biochemistry* **1989**, *28*, 2271.
101. F. von Goeler, M. Muthukumar, *J. Chem. Phys.* **1994**, *100*, 7796.
102. E. Gurovitch, P. Sens, *Phys. Rev. Lett.* **1999**, *82*, 339.
103. P. Peyser, R. Ullman, *J. Polym. Sci. A* **1965**, *3*, 3165.
104. M. Kawaguchi, H. Kawaguchi, A. Takahashi, *J. Colloid Interface Sci.* **1988**, *124*, 57.
105. J. Meadows, P. A. Williams, M. J. Garvey et al., *J. Colloid Interface Sci.* **1989**, *132*, 319.
106. R. Denoyel, G. Durand, F. Lafuma et al., *J. Colloid Interface Sci.* **1990**, *139*, 281.
107. J. Blaakmeer, M. R. Böhmer, M. A. Cohen Stuart et al., *Macromolecules* **1990**, *23*, 2301.

108. H. G. A. van de Steeg, A. de Keizer, M. A. Cohen Stuart et al., *Colloid Surf., A* **1993**, *70*, 91.
109. V. Shubin, P. Linse, *J. Phys. Chem.* **1995**, *99*, 1285.
110. N. G. Hoogeveen, Ph.D. Thesis, Wageningen Agricultural University, The Netherlands, unpublished, 1996.
111. G. J. Fleer, M. A. Cohen Stuart, J. M. H. M. Scheutjens et al., *Polymers at Interfaces*, Chapman & Hall, London, 1993, Chap. 11.
112. C. A. Haynes, W. Norde, *Colloid Surf., B* **1994**, *2*, 517.
113. P. Auroy, L. Auvray, L. Léger, *Macromolecules* **1991**, *24*, 2523.
114. O. Guiselin, L. T. Lee, B. Farnoux et al., *J. Chem. Phys.* **1991**, *95*, 4632.
115. T. Odijk, *Macromolecules* **1979**, *12*, 688.
116. A. V. Dobrynin, R. H. Colby, M. Rubinstein, *Macromolecules* **1995**, *28*, 1859.
117. H. A. van der Schee, J. Lyklema, *J. Phys. Chem.* **1984**, *88*, 6661.
118. J. Papenhuijzen, H. A. van der Schee, G. J. Fleer, *J. Colloid Interface Sci.* **1985**, *104*, 540.
119. O. A. Evers, G. J. Fleer, J. M. H. M. Scheutjens et al., *J. Colloid Interface Sci.* **1985**, *111*, 446.
120. H. G. M. van de Steeg, M. A. Cohen Stuart, A. de Keizer et al., *Langmuir* **1992**, *8*, 8.
121. P. Linse, *Macromolecules* **1996**, *29*, 326.
122. R. Varoqui, A. Johner, A. Elaissari, *J. Chem. Phys.* **1991**, *94*, 6873.
123. I. Borukhov, D. Andelman, H. Orland, *Eur. Phys. J. B* **1998**, *5*, 869.
124. I. Borukhov, D. Andelman, H. Orland, *Macromolecules* **1998**, *31*, 1665.
125. I. Borukhov, D. Andelman, H. Orland, *J. Phys. Chem. B* **1999**, *24*, 5057.
126. C. Tanford, J. C. Kirkwood, *Am. J. Chem. Soc.* **1957**, *79*, 5333.
127. D. Andelman, J. F. Joanny, *C. R. Acad. Sci. (Paris)* **2000**, *1*, 1153.
128. T. T. Nguyen, A. Y. Grosberg, B. I. Shklovskii *J. Chem. Phys.* **2000**, *113*, 1110.
129. S. J. Miklavic, S. Marcelja, *J. Phys. Chem.* **1988**, *92*, 6718.
130. S. Misra, S. Varanasi, P. P. Varanasi, *Macromolecules* **1989**, *22*, 5173.
131. P. Pincus, *Macromolecules* **1991**, *24*, 2912.
132. O. V. Borisov, T. M. Birstein, E. B. Zhulina, *J. Phys. II (France)* **1991**, *1*, 521.
133. R. S. Ross, P. Pincus, *Macromolecules* **1992**, *25*, 2177.
134. E. B. Zhulina, T. M. Birstein, O. V. Borisov, *J. Phys. II (France)* **1992**, *2*, 63.
135. J. Wittmer, J.-F. Joanny, *Macromolecules* **1993**, *26*, 2691.
136. R. Israels, F. A. M. Leermakers, G. J. Fleer et al., *Macromolecules* **1994**, *27*, 3249.
137. O. V. Borisov, E. B. Zhulina, T. M. Birstein, *Macromolecules* **1994**, *27*, 4795.
138. E. B. Zhulina, O. V. Borisov, *J. Chem. Phys.* **1997**, *107*, 5952.
139. Y. Mir, P. Auvroy, L. Auvray, *Phys. Rev. Lett.* **1995**, *75*, 2863.
140. P. Guenoun, A. Schlachli, D. Sentenac, J. M. Mays et al., *Phys. Rev. Lett.* **1995**, *74*, 3628.
141. H. Ahrens, S. Förster, C. A. Helm, *Macromolecules* **1997**, *30*, 8447.
142. H. Ahrens, S. Förster, C. A. Helm, *Phys. Rev. Lett.* **1998**, *81*, 4172.
143. S. Alexander, *J. Phys. (France)* **1977**, *38*, 983.
144. P. G. de Gennes, *Macromolecules* **1980**, *13*, 1069.
145. A. N. Semenov, *Sov. Phys. JETP* **1985**, *61*, 733.
146. S. T. Milner, T. A. Witten, M. E. Cates, *Europhys. Lett.* **1988**, *5*, 413.
147. S. T. Milner, T. A. Witten, M. E. Cates, *Macromolecules* **1988**, *21*, 2610.
148. S. T. Milner, *Science* **1991**, *251*, 905.
149. A. M. Skvortsov, I. V. Pavlushkov, A. A. Gorbunov et al., *Polym. Sci.* **1988**, *30*, 1706.
150. R. R. Netz, M. Schick, *Europhys. Lett.* **1997**, *38*, 37.
151. R. R. Netz, M. Schick, *Macromolecules* **1998**, *31*, 5105.
152. M. Murat, G. S. Grest, *Macromolecules* **1989**, *22*, 4054.
153. A. Chakrabarti, R. Toral, *Macromolecules* **1990**, *23*, 2016.
154. P. Y. Lai, K. Binder, *J. Chem. Phys.* **1991**, *95*, 9288.
155. C. Seidel, R. R. Netz, *Macromolecules* **2000**, *33*, 634.
156. F. S. Csajka, C. Seidel, *Macromolecules* **2000**, *33*, 2728.
157. F. S. Csajka, R. R. Netz, C. Seidel et al., *Eur. Phys. J. E* **2001**, *4*, 505.